

Article

Integrative Descriptions of Two New *Mesobiotus* Species (Tardigrada, Eutardigrada, Macrobiotidae) from Vietnam [†]

Daniel Stec ^{1,2} 

¹ Institute of Systematics and Evolution of Animals, Polish Academy of Sciences, Sławkowska 17, 31-016 Kraków, Poland; daniel.stec@isez.pan.krakow.pl

² Department of Invertebrate Evolution, Institute of Zoology and Biomedical Research, Faculty of Biology, Jagiellonian University, Gronostajowa 9, 30-387 Kraków, Poland

[†] urn:lsid:zoobank.org:act:6ABF8C3D-FDD1-4DE0-88C8-54F49E21EFB4 (*Mesobiotus imperialis* sp. nov.); urn:lsid:zoobank.org:act:26C5E830-9A84-4019-B3A4-301339FE3220 (*Mesobiotus marmoreus* sp. nov).

Abstract: To date, 34 tardigrade taxa have been recorded from Vietnam and this includes only two macrobiotid species belonging to the genus *Mesobiotus*. In this paper, two additional species of this genus, one of the *M. harmsworthi* group and one of the *M. furciger* group, are reported and described as new for science (*Mesobiotus imperialis* sp. nov., *Mesobiotus marmoreus* sp. nov.). Both descriptions have an integrative character providing detailed morphological and morphometric data collected by phase contrast and scanning electron microscopy that are linked to genetic data. The latter constitute DNA sequences of molecular markers that are commonly used in tardigrade taxonomy. The genus phylogeny is also provided, elucidating the phylogenetic position of the newly discovered taxa.

Keywords: *Mesobiotus harmsworthi* group; *Mesobiotus furciger* group; morphogroup; new species; tardigrades; taxonomy; phylogeny



Citation: Stec, D. Integrative Descriptions of Two New *Mesobiotus* Species (Tardigrada, Eutardigrada, Macrobiotidae) from Vietnam. *Diversity* **2021**, *13*, 605. <https://doi.org/10.3390/d13110605>

Academic Editor: Michael Wink

Received: 2 November 2021

Accepted: 16 November 2021

Published: 21 November 2021

Publisher's Note: MDPI stays neutral with regard to jurisdictional claims in published maps and institutional affiliations.



Copyright: © 2021 by the author. Licensee MDPI, Basel, Switzerland. This article is an open access article distributed under the terms and conditions of the Creative Commons Attribution (CC BY) license (<https://creativecommons.org/licenses/by/4.0/>).

1. Introduction

Tardigrades, also known as water bears, are a phylum of microscopic animals whose body size usually does not exceed 1 mm. These organisms are ubiquitous as they are found in marine, freshwater and various limno-terrestrial habitats all over the world [1]. To date, more than 1300 species have been formally described and, interestingly, a great majority of them were found in mosses and lichens [2–4].

The genus *Mesobiotus* was founded five years ago by Vecchi et al. [5] based on morphological distinctions from other genera within Macrobiotidae. The composition was further supported by phylogenetic analyses confirming the newly proposed taxon to be monophyletic [5] and, as such, was also recovered in the recent phylogeny of the family Macrobiotidae [6]. Now, the genus comprises 71 nominal species that are grouped into two unformal complexes, namely the *Mesobiotus harmsworthi* group and the *Mesobiotus furciger* group [4,7,8]. Although this morphological clustering of *Mesobiotus* taxa helps other researchers in taxonomic studies devoted to these macrobiotids, it has been demonstrated that the grouping does not reflect the phylogenetic relationship within the genus [6,7,9]. Out of 34 species representing the currently known tardigrade fauna of Vietnam [10–16], only two belong to the genus *Mesobiotus*. The first one is *Mesobiotus harmsworthi* (Murray, 1907) [17], the type species for the genus, as well as the recently discovered *Mesobiotus datanlanicus* Stec, 2019 [15]. Notably, according to the recent redescription the occurrence of *M. harmsworthi* in Vietnam, it should be treated with great caution [9].

In the present study, two new *Mesobiotus* species are described by means of an integrative taxonomy approach. Both descriptions comprise detailed morphological and morphometric data collected under phase contrast and scanning electron microscopy (PCM and SEM, respectively). Furthermore, phenotypic data DNA sequences of molecular mark-

ers used as a standard in tardigrade taxonomy are provided for each analysed species. Finally, the phylogenetic tree presenting the position of both new taxa is also presented.

2. Material and Methods

2.1. Sample Processing

Two moss samples containing new species were collected in Hué and in the Marble Mountains, south of Đà Nẵng city (Vietnam). The samples were collected by Daniel Stec and Krzysztof Miler in August 2018 from tree bark and a stone walkway, respectively. The samples were examined for terrestrial tardigrades using standard methods (e.g., Stec et al. [18]). A total of 75 and 56 animals as well as 55 and 13 eggs of the two new species were extracted from both samples, respectively. In order to perform integrative taxonomic descriptions, the isolated animals and eggs were split into three groups for specific analyses: Morphological analysis with phase contrast light microscopy, morphological analysis with scanning electron microscopy and DNA sequencing (for details please see sections “Material examined” provided below for each description).

2.2. Microscopy and Imaging

Specimens for light microscopy were mounted on microscope slides in a small drop of Hoyer’s medium and secured with a cover slip, following the protocol by Morek et al. [19]. Slides were then dried for five to seven days at 60 °C. Dried slides were sealed with a transparent nail polish and examined under an *Olympus BX53* light microscope with phase contrast (PCM), as well as with an *Olympus DP74* digital camera. Immediately after mounting the specimens in the medium, slides were checked under PCM for the presence of males and females in the studied population, as the spermatozoa in testis and *vas deferens* are visible only for several hours after mounting [20,21]. In order to obtain clean eggs for SEM, eggs were processed according to the protocol by Stec et al. [18]. In short, eggs were first subjected to a water/ethanol and an ethanol/acetone series, then to CO₂ critical-point drying and finally sputter-coated with a thin layer of gold. Specimens were examined under high vacuum in a *Versa 3D DualBeam* Scanning Electron Microscope at the ATOMIN facility of the Jagiellonian University, Kraków, Poland. All figures were assembled in *Corel Photo-Paint X6*. For structures that could not be satisfactorily focused on in a single photograph, a stack of 2–6 images were taken with an equidistance of ca. 0.2 µm and assembled manually into a single deep-focus image.

2.3. Morphometrics and Morphological Nomenclature

All measurements are given in micrometres (µm). Sample size was adjusted following recommendations by Stec et al. [22]. Structures were measured only if their orientation was suitable. Body length was measured from the anterior extremity to the end of the body, excluding the hind legs. The buccal apparatus and claws were classified according to Pilato and Binda [23] and Vecchi et al. [5], respectively. The terminology used to describe the oral cavity armature and the egg-shell morphology follows Michalczyk and Kaczmarek [24] and Kaczmarek and Michalczyk [25]. The macroplacoid length sequence is given according to Kaczmarek et al. [26] whereas morphological states of cuticular bars on legs follow Kiosya et al. [27]. The buccal tube length and the level of the stylet support insertion point were measured according to Pilato [28]. The *pt* index is the ratio of the length of a given structure to the length of the buccal tube expressed as a percentage (Pilato 1981). All other measurements and nomenclature follow Kaczmarek and Michalczyk [25]. The buccal tube width was measured as the external and internal diameter at the level of the stylet support insertion point. The lengths of the claw branches were measured from the base of the claw (i.e., excluding the lunula) to the top of the branch, including accessory points. The distance between egg processes was measured as the shortest distance between the base edges of the two closest processes. Morphometric data were handled using the “Parachela” ver. 1.8 template available from the Tardigrada Register [29] and are given in Supplementary Materials (SM.1 and SM.2). T-test comparisons of morphometric characters

of one of the new species and *Mesobiotus philippinicus* Mapalo, Stec, Mirano-Boscós & Michalczyk, 2016 [30] were conducted using the statistical programming language R [31]. Since multiple testing inflates the Type I error rate, the Benjamini–Hochberg correction to the α -level was applied [32] independently to each of the three sets of *t*-tests (absolute and relative animal measurements as well as egg measurements). Results of the *t*-tests are given in Supplementary Materials (SM.3). The taxonomic keys for the genus *Mesobiotus* by Kaczmarek et al. [7] and Tumanov [8] were used to determine whether the isolated species had previously been described. The tardigrade taxonomy follows Stec et al. [6].

2.4. DNA Sequencing

The DNA was extracted from individual animals following a *Chelex*[®] 100 resin (*Bio-Rad*) extraction method by Casquet et al. [33] with modifications described in detail in Stec et al. [34]. Four DNA fragments differing in mutation rates were sequenced. Namely, the small ribosome subunit (18S rRNA, nDNA), the large ribosome subunit (28S rRNA, nDNA), the internal transcribed spacer (ITS-2, nDNA), and the cytochrome oxidase subunit I (COI, mtDNA). All fragments were amplified and sequenced according to the protocols described in Stec et al. [34]; primers are listed in Table 1. Sequencing products were read with the *ABI 3130xl* sequencer at the Molecular Ecology Lab, Institute of Environmental Sciences of the Jagiellonian University, Kraków, Poland. Sequences were processed in *BioEdit* ver. 7.2.5 [35] and submitted to GenBank. Prior to submission, all obtained COI sequences were translated into protein sequences in *MEGA7* version 7.0 [36] to check against pseudogenes.

Table 1. Primers with their original references used for amplification of the four DNA fragments sequenced in the study.

DNA Marker	Primer Name	Primer Direction	Primer Sequence (5'-3')	Primer Source
18S rRNA	18S_Tar_Ff1	forward	AGGCGAAACCGCGAATGGCTC	[37]
	18S_Tar_Rr1	reverse	GCCGCAGGCTCCACTCCTGG	
28S rRNA	28S_Eutar_F	forward	ACCCGCTGAACTTAAGCATAT	[38]
	28SR0990	reverse	CCTTGGTCCGTGTTTCAAGAC	[39]
ITS-2	ITS2_Eutar_Ff	forward	CGTAACGTGAATTGCAGGAC	[40]
	ITS2_Eutar_Rr	reverse	TCCTCCGCTTATTGATATGC	
COI	LCO1490-JJ	forward	CHACWAAYCATAAAGATATYGG	[41]
	HCO2198-JJ	reverse	AWACTTCVGGRTGVCCAAARAATCA	

2.5. Phylogenetic Analysis and Genetic Comparisons

To establish phyletic positions of both new species, a phylogenetic tree was constructed using the dataset from Kaczmarek et al. [7] with the addition of sequences obtained in this study as well as sequences that were published to date (Table 2). DNA sequences of *Macrobiotus kamilae* Coughlan & Stec, 2019 [20] and *Macrobiotus hanna*e Nowak & Stec, 2018 [42] were used as the outgroup. The sequences were aligned using the AUTO method (for COI and ITS-2) and the Q-INS-I method (for ribosomal markers: 18S rRNA and 28S rRNA) of MAFFT version 7 [43,44] and manually checked against non-conservative alignments in BioEdit. Then, the aligned sequences were trimmed to 1016 (18S rRNA), 811 (28S rRNA), 554 (ITS-2), and 658 (COI) bp and concatenated using SequenceMatrix [45]. Before partitioning, the concatenated alignment was divided into 6 data blocks constituting three separate blocks of ribosomal markers and three separate blocks of three codon positions in the COI dataset. Using PartitionFinder [46] under the Akaike Information Criterion (AIC), the best scheme of partitioning and substitution models were chosen for posterior phylogenetic analysis (SM.04). Bayesian inference (BI) marginal posterior probabilities were calculated for the concatenated (18S rRNA + 28S rRNA + ITS-2 + COI) dataset using MrBayes v3.2 [47]. Random starting trees were used, and the analysis was run for 10 million generations, sampling the Markov chain every 1000 generations. An average standard deviation of split frequencies of <0.01 was used as a guide to ensure the

two independent analyses had converged. The program Tracer v1.6 [48] was then used to ensure Markov chains had reached stationarity, and to determine the correct 'burn-in' for the analysis, which was the first 10% of generations. The ESS values were greater than 200 and the consensus tree was obtained after summarising the resulting topologies and discarding the 'burn-in'. The consensus tree was viewed and visualised by FigTree v.1.4.3 available from <http://tree.bio.ed.ac.uk/software/figtree> (accessed on 10 August 2018). Uncorrected pairwise distances were calculated using MEGA7 and are given in Supplementary Materials (SM.5).

Table 2. Sequences used for phylogenetic analysis and genetic comparisons (see Material and Methods section for details). Bold font indicates sequences obtained in this study.

Species	18S rRNA	28S rRNA	ITS-2	COI	Source
<i>M. ethiopicus</i> Stec & Kristensen, 2017 [49]	MF678793	MF678792	MN122776	MF678794	[15,49]
<i>M. datanlanicus</i> Stec, 2019 [15]	MK584659	MK584658	MK584657	MK578905	[15]
<i>M. dilimanensis</i> Itang et al., 2020 [50]	MN257048	MN257049	MN257050	MN257047	[50]
<i>M. philippinicus</i> Mapalo et al., 2016 [30]	KX129793	KX129794	KX129795	KX129796	[30]
<i>M. insanis</i> Mapalo et al., 2017 [51]	MF441488	MF441489	MF441490	MF441491	[51]
<i>M. hilariae</i> Vecchi et al., 2016 [5]	KT226070			KT226108	[5]
<i>M. radiatus</i> (Pilato et al., 1991) [52]	MH197153	MH197152	MH197267	MH195147	[53]
			MH197268	MH195148	
<i>M. romani</i> Roszkowska et al., 2018 [54]	MH197158	MH197151	MH197150	MH195149	[54]
<i>M. harmsworthi</i> (Murray, 1907) [17]	MH197146	MH197264	MH197154	MH195150	[9]
				MH195151	
<i>M. occultatus</i> Kaczmarek et al., 2018 [9]	MH197147		MH197155	MH195152	[9]
<i>M. furciger</i> group species NO	MH197148	MH197265	MH197156	MH195153	[9]
<i>M. harmsworthi</i> group species RU	MH197149	MH197266	MH197157	MH195154	[9]
<i>M. furciger</i> (Murray, 1907) [55]				JX865306	[56]
				JX865308	
				JX865314	
<i>M. fiedleri</i> Kaczmarek et al., 2020 [7]	MH681585	MH681693	MH681724	MH676056	[7]
" <i>M. harmsworthi</i> "				GU113140	Li and Xiao (unpublished)
<i>M. anastasiae</i> Tumanov, 2020 [8]	MT903468	MT903612	MT903470	MT904513	[8]
<i>M. skoracki</i> Kaczmarek et al., 2018 [9]		MW680636		MW656257	[57]
<i>M. imperialissp. nov.</i>	OL257854	OL257866		OL311514	this study
	OL257855	OL257867		OL311515	this study
<i>M. marmoreussp. nov.</i>	OL257856	OL257868	OL257861	OL311516	this study
	OL257857	OL257869	OL257862	OL311517	this study
	OL257858	OL257870	OL257863	OL311518	this study
<i>M. cf. barabanovi</i>	MN310392	MN310388	MN310390	MN313170	[7]
<i>Macrobiotus kamilae</i> Coughlan & Stec, 2019 [20]	MK737070	MK737064	MK737067	MK737920	[20]
				MK737921	
<i>Macrobiotus hanna</i> e Nowak & Stec, 2018 [42]	MH063922	MH063924	MH063923	MH057764	[42]

3. Results

3.1. Taxonomic Account of the New Species

Phylum: Tardigrada Doyère, 1840 [58].

Class: Eutardigrada Richters, 1926 [59].

Order: Parachela Schuster, Nelson, Grigarick & Christenberry, 1980 [60].

Superfamily: Macrobiotioidea Thulin, 1928 [61] (in [62]).

Family: Macrobiotidae Thulin, 1928 [61].

Genus: *Mesobiotus* Vecchi, Cesari, Bertolani, Jönsson, Rebecchi & Guidetti, 2016 [5].

3.2. Description of the New Species

***Mesobiotus imperialis* sp. nov.**

ZooBank: urn:lsid:zoobank.org:act:6ABF8C3D-FDD1-4DE0-88C8-54F49E21EFB4

(Tables 3 and 4, Figures 1–6).

Table 3. Measurements [in μm] and *pt* values of selected morphological structures of animals of *Mesobiotus imperialis* sp. nov.; specimens mounted in Hoyer's medium; N—number of specimen/structures measured, RANGE refers to the smallest and the largest structure among all measured specimens; SD—standard deviation.

CHARACTER	N	RANGE					Mean		SD		Holotype		
		μm	μm	μm	μm	μm	<i>pt</i>	μm	<i>pt</i>	μm	<i>pt</i>		
Body length	20	313	–	539	895	–	1219	389	1012	51	75	436	1053
Buccal tube													
Buccal tube length	20	30.5	–	44.2		–		38.4	–	3.4	–	41.4	–
Stylet support insertion point	20	22.9	–	34.1	75.0	–	77.3	29.2	76.0	2.7	0.8	31.2	75.4
Buccal tube external width	20	5.2	–	7.6	15.7	–	18.1	6.5	16.8	0.6	0.6	7.0	16.9
Buccal tube internal width	20	4.0	–	5.7	10.8	–	13.8	4.9	12.6	0.5	0.7	5.7	13.8
Ventral lamina length	20	19.9	–	27.0	56.2	–	65.2	23.2	60.4	1.8	2.2	23.6	57.0
Placoid lengths													
Macroplacoid 1	20	3.8	–	6.0	11.7	–	14.4	5.1	13.4	0.6	0.9	5.6	13.5
Macroplacoid 2	20	2.9	–	4.5	7.7	–	11.3	3.7	9.7	0.5	0.9	4.2	10.1
Macroplacoid 3	20	3.1	–	5.8	10.2	–	13.1	4.5	11.6	0.6	0.8	4.7	11.4
Microplacoid	20	3.2	–	5.2	8.3	–	12.7	4.1	10.7	0.5	1.1	4.2	10.1
Macroplacoid row	20	11.9	–	19.4	38.6	–	43.9	16.0	41.5	1.8	1.6	17.9	43.2
Placoid row	20	16.0	–	25.7	52.0	–	58.5	21.3	55.4	2.4	2.2	23.8	57.5
Claw I heights													
External primary branch	20	7.5	–	10.6	20.7	–	25.6	8.7	22.8	0.8	1.4	9.6	23.2
External secondary branch	18	6.4	–	8.5	17.2	–	22.3	7.3	19.0	0.7	1.5	7.9	19.1
Internal primary branch	20	6.7	–	10.0	19.7	–	22.6	8.2	21.2	0.9	0.9	9.2	22.2
Internal secondary branch	18	5.1	–	8.0	15.8	–	19.2	6.7	17.3	0.7	1.1	7.4	17.9
Claw II heights													
External primary branch	20	7.3	–	11.1	22.3	–	26.0	9.2	24.0	0.9	1.0	10.3	24.9
External secondary branch	18	6.6	–	8.8	17.6	–	22.9	7.6	19.9	0.7	1.5	7.3	17.6
Internal primary branch	20	7.2	–	9.6	19.2	–	23.6	8.1	21.2	0.7	1.2	8.6	20.8
Internal secondary branch	13	6.1	–	8.0	16.4	–	20.3	7.1	18.4	0.6	1.4	7.1	17.1
Claw III heights													
External primary branch	20	7.8	–	11.1	21.4	–	27.9	9.3	24.2	0.9	1.6	10.4	25.1
External secondary branch	18	6.4	–	8.8	17.2	–	23.1	7.6	19.8	0.7	1.6	8.8	21.3
Internal primary branch	19	6.0	–	9.7	16.2	–	23.3	8.0	20.9	1.0	1.6	8.5	20.5
Internal secondary branch	15	5.9	–	8.1	16.9	–	20.8	7.1	18.3	0.7	1.1	8.0	19.3
Claw IV heights													
Anterior primary branch	20	8.0	–	11.2	23.4	–	28.2	9.7	25.3	0.9	1.2	10.8	26.1
Anterior secondary branch	18	6.5	–	8.8	17.9	–	22.1	7.8	20.3	0.7	1.1	8.5	20.5
Posterior primary branch	20	8.5	–	12.1	25.0	–	30.1	10.3	27.0	0.9	1.2	11.0	26.6
Posterior secondary branch	9	7.7	–	9.3	20.2	–	22.1	8.3	21.2	0.5	0.7	?	?

Table 4. Measurements [in μm] of the eggs of *Mesobiotus imperialis* sp. nov.; eggs mounted in Hoyer's medium; process base/height ratio is expressed as percentage; N—number of eggs/structures measured, RANGE refers to the smallest and the largest structure among all measured specimens; SD—standard deviation.

Character	N	RANGE		Mean		SD
Egg bare diameter	20	53.9	–	70.2	62.8	4.0
Egg full diameter	20	74.7	–	94.6	85.7	4.9
Process height	60	8.3	–	15.3	11.9	1.3
Process base width	60	6.9	–	12.5	10.0	1.1
Process base/height ratio	60	65%	–	116%	85%	11%
Inter-process distance	60	1.7	–	3.9	2.7	0.5
Number of processes on the egg circumference	20	15	–	18	16.2	0.8

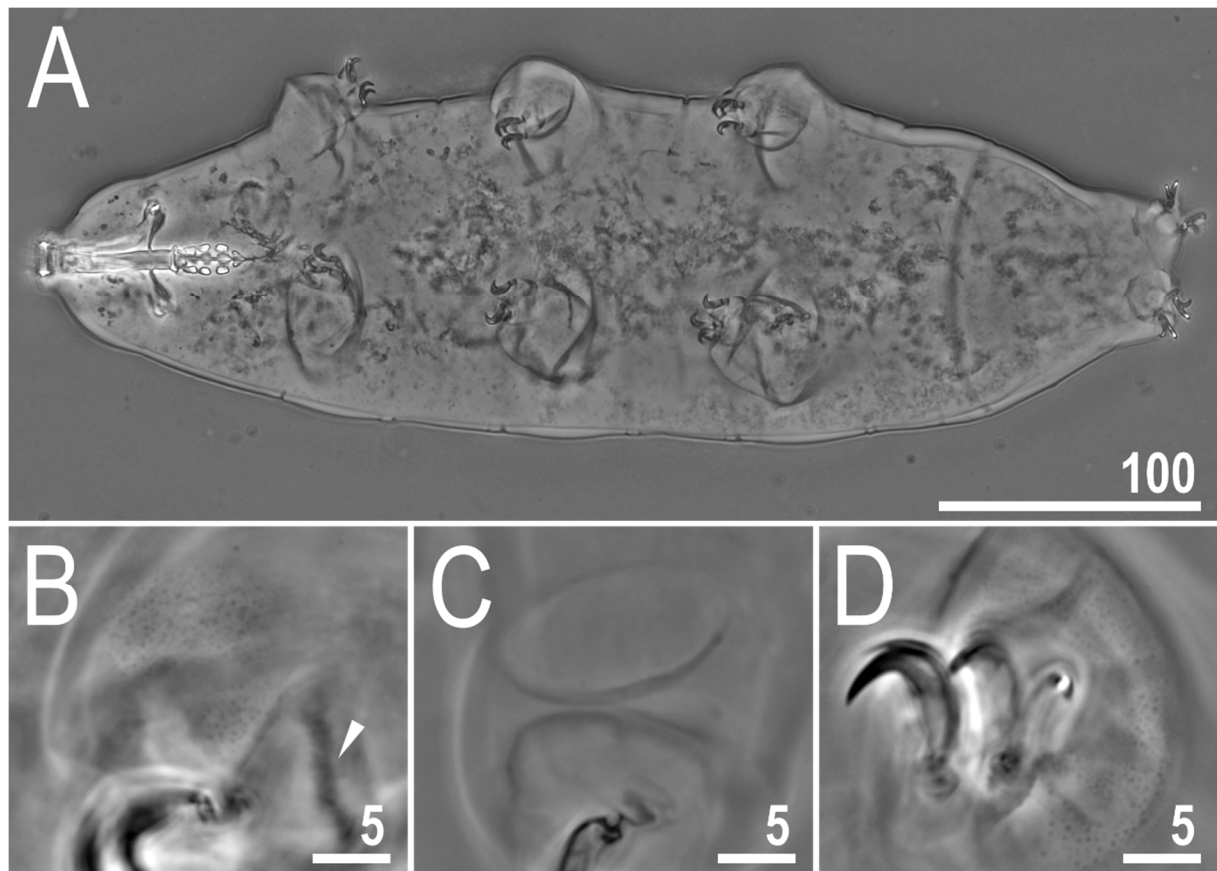


Figure 1. *Mesobiotus imperialis* sp. nov.—PCM image of habitus and leg's cuticle morphology: (A)—dorso-ventral projection (holotype); (B)—granulation on the external surface of leg II (holotype); (C)—a pulvinus-like cuticular bulge on the internal surface of leg III (paratype); (D)—granulation on dorsal and lateral surface of leg IV (paratype). Filled flat arrowhead indicates a single continuous cuticular bar above the claws. Scale bar in μm .

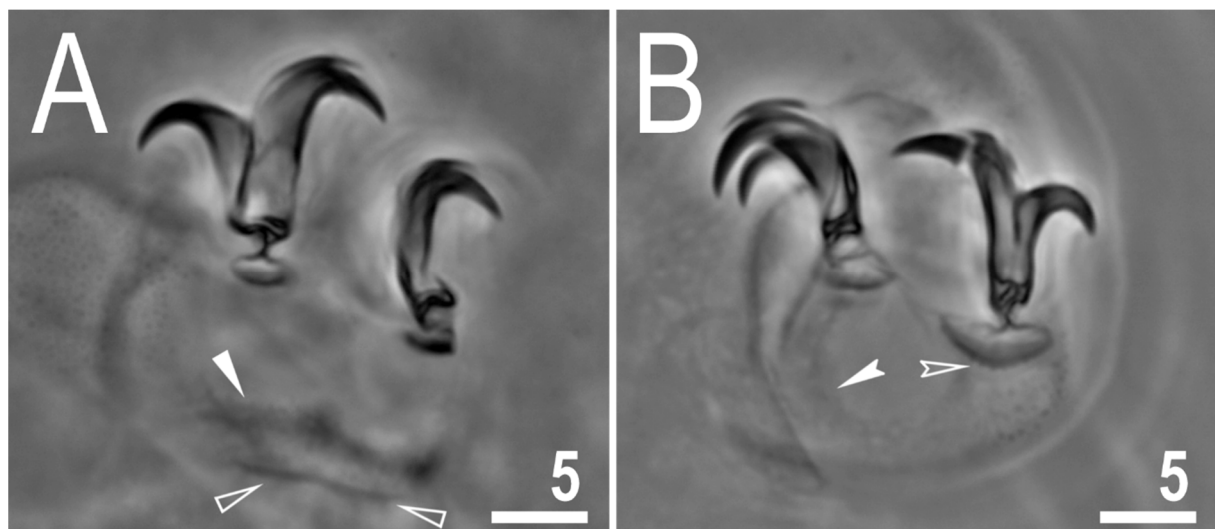


Figure 2. *Mesobiotus imperialis* sp. nov.—PCM images of claws: (A)—claw III with smooth lunulae (holotype); (B)—claw IV with smooth lunulae (paratype). Filled flat arrowhead indicates a single continuous cuticular bar above the claws, empty flat arrowheads indicate paired muscles attachments, filled indented arrowhead indicates horseshoe structure connecting the anterior and the posterior claw, empty indented arrowheads indicate faint dentation in lunula IV. Scale bars in μm .

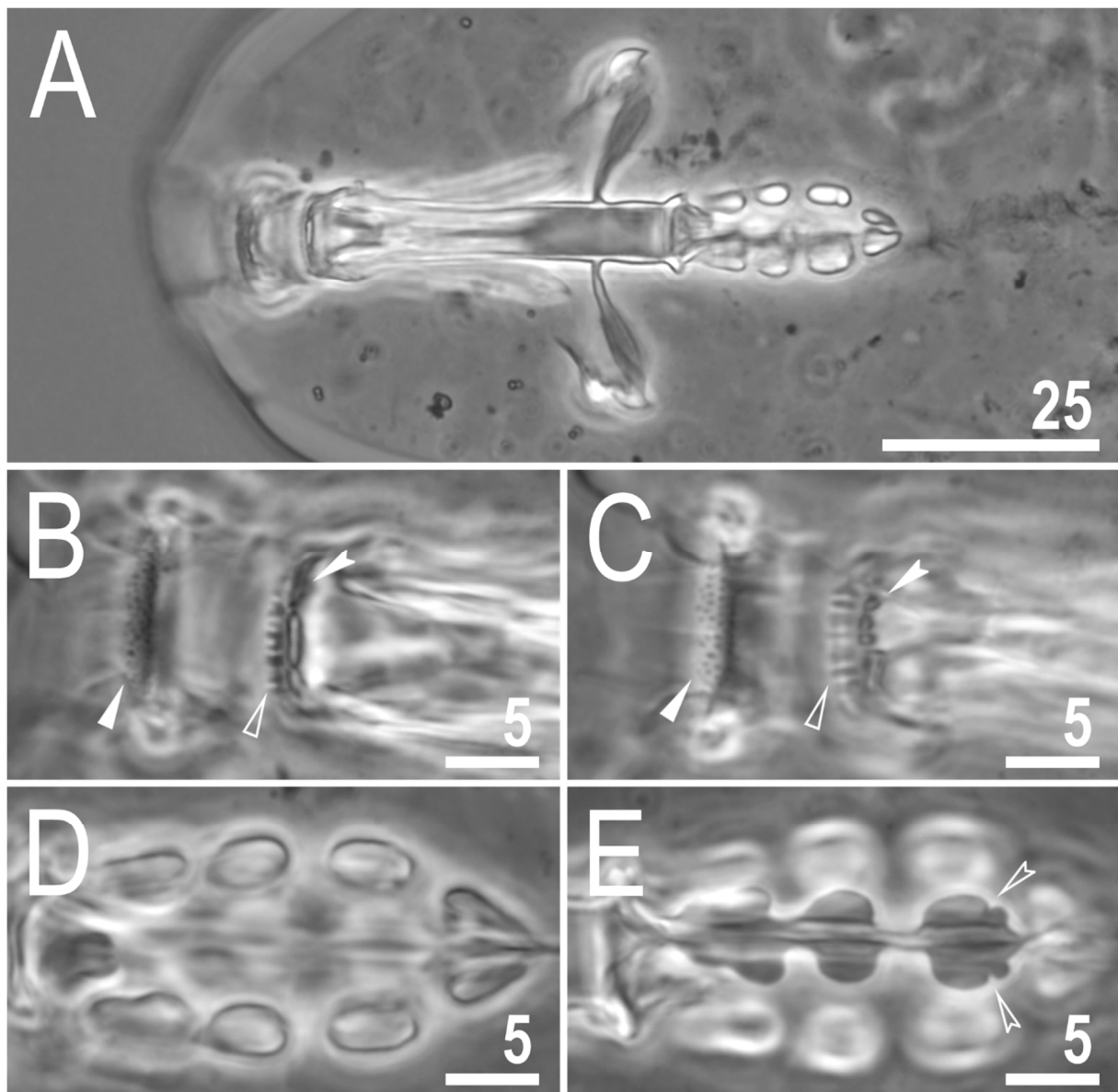


Figure 3. *Mesobiotus imperialis* sp. nov.—PCM images of the buccal apparatus: (A)—an entire buccal apparatus (paratype); (B,C)—the oral cavity armature, dorsal and ventral teeth, respectively (paratype); (D,E)—placoid morphology, dorsal and ventral placoids, respectively (holotype). Filled flat arrowheads indicate the first band of teeth, empty flat arrowheads indicate the second band of teeth, filled indented arrowheads indicate the third band of teeth, empty indented arrowheads indicate subterminal constrictions in the third macroplacoid. Scale bars in μm .

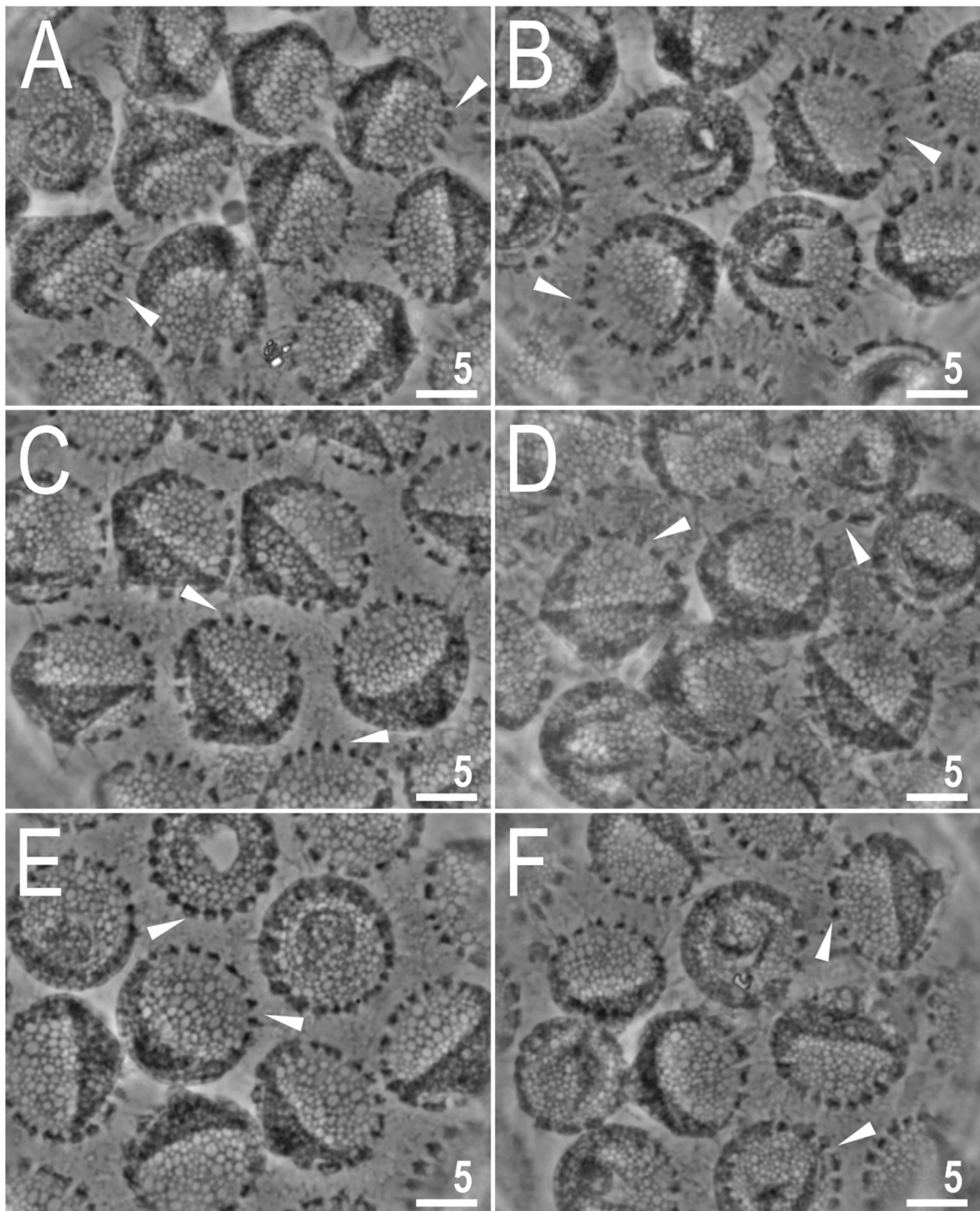


Figure 4. *Mesobiotus imperialis* sp. nov.—PCM images of the egg surface under $\times 1000$ magnification. Arrowheads indicate crowns of strong thickenings around the process bases. Scale bars in μm .

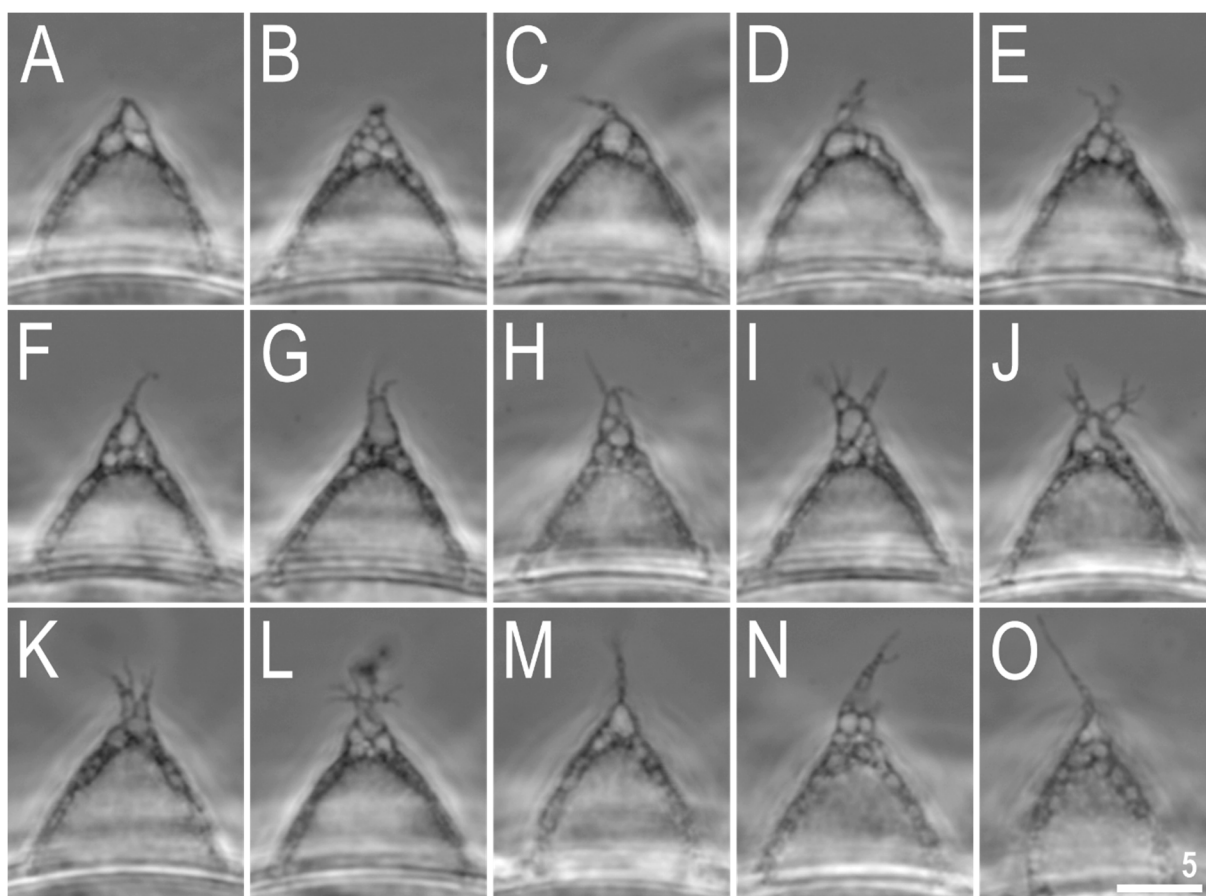


Figure 5. *Mesobiotus imperialis* sp. nov.—PCM images of the egg processes midsections under $\times 1000$ magnification. Scale bar in μm .

3.2.1. Material Examined

In total, 73 animals, 50 eggs mounted on microscope slides in Hoyer's medium (some of the eggs were embryonated), 5 eggs fixed on a SEM stub (19.14) and 2 specimens were processed for DNA sequencing.

3.2.2. Type Locality

$16^{\circ}28'04''$ N, $107^{\circ}34'37''$ E; 6 m asl: Vietnam, Huế, Imperial City, Kiến Trung Palace (Điện Kiến Trung), bark of a dying tree near a pat walk, coll. Daniel Stec and Krzysztof Miler, August 2018.

3.2.3. Etymology

The species is named after the place where it was discovered. Namely, it is Imperial City, a walled enclosure within the citadel of the city of Huế and the former imperial capital of Vietnam.

3.2.4. Type Depositories

The holotype with 6 paratypes (slide VN.061.03) and 47 paratypes (slides: VN.061.*, where the asterisk can be substituted by any of the following numbers: 01–02, 04–09) and 26 eggs (slides: VN.061.*: 12–15) are deposited at the Institute of Systematics and Evolution of Animals, Polish Academy of Sciences, Sławkowska 17, 31-016, Kraków, Poland;

Nineteen paratypes (slides: VN.061.*: 10–11), 24 eggs (slides: VN.061.*: 16–17) and SEM stub: 19.14 are deposited at the Institute of Zoology and Biomedical Research, Jagiellonian University, Gronostajowa 9, 30-387, Kraków, Poland.

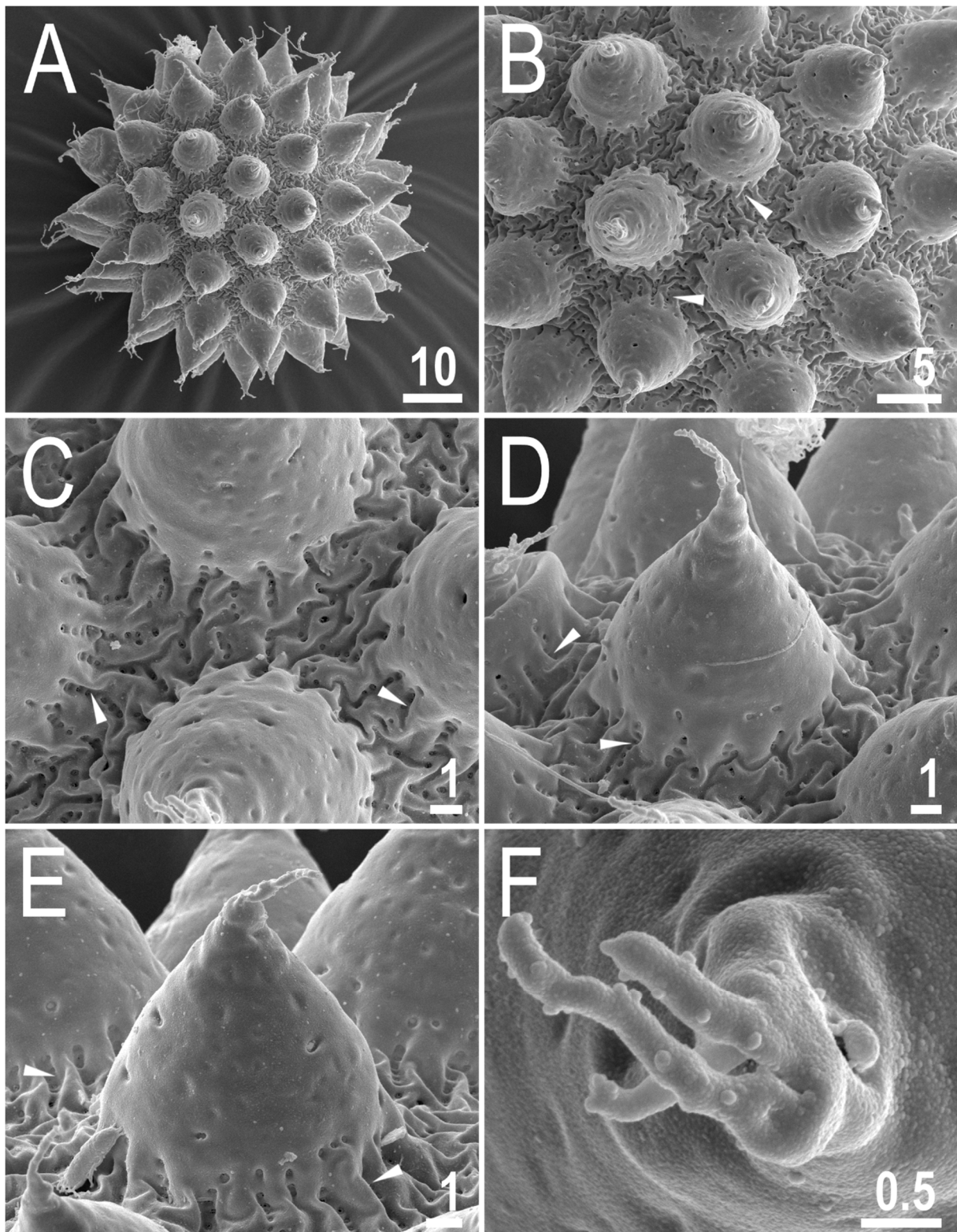


Figure 6. *Mesobiotus imperialis* sp. nov.—SEM images of eggs: (A)—entire view of the egg; (B,C)—details of the egg surface between processes; (D,E)—egg processes; (F)—top part of the processes divided into several flexible filaments covered with fine granulation. Arrowheads indicate strong thickenings around the process bases. Scale bars in μm .

3.2.5. Animals

The body is almost transparent in small specimens and whitish in adults; after fixation in Hoyer's medium, the body is transparent (Figure 1A). Eyes are present in alive animals and dissolved by Hoyer's medium in about 50% of all mounted specimens. The body cuticle is smooth, i.e., without pores or sculpturing. Fine granulation is present on the external surface of all legs I–III (Figure 1B) as well as on the lateral and dorsal surfaces of legs IV (Figure 1D). A cuticular bulge/fold, resembling a pulvinus, is present on the internal surface of legs I–III (Figure 1C). Claws of the *Mesobiotus* type were observed, with a peduncle connecting the claw to the lunula, a basal septum and well-developed accessory points situated in parallel to the primary branch (Figure 2A,B). Lunulae under claws I–III are smooth (Figure 2A) and those under claws IV are slightly dentate (Figure 2B; a character visible in about 50% of specimens mounted in Hoyer's medium). A single continuous cuticular bar and double muscle attachments are present above claws I–III (Figures 1B and 2A), whereas a horseshoe-shaped structure connects the anterior and posterior lunulae on claws IV (Figure 2B).

The mouth is antero-ventral. The Bucco-pharyngeal apparatus is of the *Macrobiotus* type, with the ventral lamina and ten small peribuccal lamellae (Figure 3A). The oral cavity armature is well developed and is composed of three bands of teeth (Figure 3B,C). The first band of teeth is composed of numerous small granules arranged in several discrete rows situated anteriorly in the oral cavity, just behind the bases of the peribuccal lamellae (Figure 3B,C). The second band of teeth is situated between the ring fold and the third band of teeth and is composed of ridges parallel to the main axis of the buccal tube that are larger than those in the first band (Figure 3B,C). The teeth of the third band are located within the posterior portion of the oral cavity, between the second band of teeth and the buccal tube opening (Figure 3B,C). The third band of teeth is discontinuous and divided into dorsal and ventral portions. Under PCM, dorsal teeth are visible as two lateral and one median transverse ridges/crests (Figure 3B) whereas ventral teeth consist of two lateral transverse ridges/crests, between which two to four (usually three) roundish and separated ventro-median teeth are present (Figure 3C). The pharyngeal bulb is ovoid (Figure 3A), with triangular apophyses, three rod-shaped macroplacoids and a large, elongated drop-shaped microplacoid placed close to the third macroplacoid (Figure 3D,E). The macroplacoid length sequence is $2 < 3 < 1$. The first macroplacoid is anteriorly narrowed and the third has a clearly defined sub-terminal constriction (Figure 3E). Measurements and statistics are presented in Table 3.

3.2.6. Eggs

Eggs are white, laid free, spherical in shape and equipped with conical processes (Figures 4–6). In PCM, the egg surface between processes seems to be rough with both dark and faintly light refracting dots (Figure 4), whereas in SEM, the surface is clearly wrinkled, with wrinkles radiating out from the process bases but not forming a connective network (Figure 6A–E). Small pores (up to 0.3 μm) are scattered across the inter-process surface with their lumen often being covered by a reticulate internal structure that seems to be a remnant of the reduced labyrinthine layer. The pores are clearly visible in SEM (Figure 6A–E), but under PCM, they are most probably seen as the mentioned faintly light refracting dots (Figure 4). The bases of egg processes are surrounded by crowns of strong thickenings that are evident in PCM as well as SEM (Figures 4 and 6A–E). The egg processes are evenly spaced, with a flexible upper portion often equipped with shorter flexible filaments (Figure 5). This flexible portion of the processes seems to be fragile and susceptible to fracture (Figure 5A–C). Often, in the upper portion of the egg processes, below the flexible part, a bubble-like structure is present and visible in the process midsection (Figure 5). The labyrinthine layer is visible under PCM as a reticulum in process walls, with varying mesh sizes uniformly distributed within the process walls (Figure 4). In SEM, the process walls are smooth with unevenly distributed depressions and faint tubercles and occasionally also pores often with closed lumen (Figure 6A–E). The top flexible portions of egg processes

are irregularly covered with small granules that are visible only in SEM (Figure 6D,F). Measurements and statistics are presented in Table 4.

3.2.7. Reproduction

The examination of all individuals, freshly mounted in Hoyer's medium, under PCM did not reveal any testis or spermathecae filled with spermatozoa. Thus, it is most likely that the new species is parthenogenetic.

3.2.8. DNA sequences

The obtained sequences for three molecular markers analysed in this study were of good quality and were represented by single haplotypes. However, several attempts to amplify the ITS-2 marker for the new species failed, preventing me from obtaining these sequences for the new species.

The **18S rRNA** sequences (GenBank: OL257854-5), 1008 bp long.

The **28S rRNA** sequences (GenBank: OL257866-7), 774 bp long.

The **COI** sequences (GenBank: OL311514-5), 658 bp long.

3.3. Description of the New Species

Mesobiotus marmoreus sp. nov.

ZooBank: urn:lsid:zoobank.org:act:26C5E830-9A84-4019-B3A4-301339FE3220

(Tables 5 and 6, Figures 7–11).

Table 5. Measurements [in μm] and *pt* values of selected morphological structures of animals of *Mesobiotus marmoreus* sp. nov.; specimens mounted in Hoyer's medium; N—number of specimen/structures measured, RANGE refers to the smallest and the largest structure among all measured specimens; SD—standard deviation.

Character	N	RANGE					Mean		SD		Holotype		
		μm	μm	μm	μm	μm	pt	μm	pt	μm	pt		
Body length	20	234	–	372	883	–	1042	320	970	32	48	308	982
Buccal tube													
Buccal tube length	20	26.5	–	37.1		–	33.0	–	2.7	–	31.3	–	
Stylet support insertion point	20	20.2	–	28.7	76.2	–	77.8	25.5	77.1	2.2	0.5	24.0	76.7
Buccal tube external width	20	4.5	–	6.4	16.2	–	18.4	5.6	17.0	0.5	0.6	5.3	16.9
Buccal tube internal width	20	3.2	–	4.9	12.0	–	14.6	4.2	12.7	0.4	0.6	3.9	12.5
Ventral lamina length	20	15.9	–	22.5	57.9	–	62.5	19.9	60.2	1.6	1.1	19.2	61.3
Placoid lengths													
Macroplacoid 1	20	3.6	–	6.1	12.9	–	16.4	4.8	14.6	0.6	0.9	4.2	13.4
Macroplacoid 2	20	2.3	–	3.8	8.5	–	10.8	3.2	9.6	0.4	0.6	3.0	9.6
Macroplacoid 3	20	3.2	–	5.0	10.6	–	13.6	4.0	12.0	0.6	1.1	3.4	10.9
Microplacoid	20	3.0	–	4.7	9.6	–	12.7	3.6	10.9	0.4	0.8	3.5	11.2
Macroplacoid row	20	11.1	–	16.9	38.9	–	45.6	14.0	42.4	1.5	1.6	12.6	40.3
Placoid row	20	15.0	–	22.7	53.7	–	61.2	18.8	56.7	1.9	1.8	17.3	55.3
Claw I heights													
External primary branch	20	6.4	–	8.6	19.5	–	25.4	7.6	23.0	0.6	1.5	7.7	24.6
External secondary branch	16	5.1	–	7.6	15.5	–	20.9	6.3	18.9	0.6	1.4	6.2	19.8
Internal primary branch	20	6.2	–	8.4	18.9	–	24.2	7.3	22.1	0.6	1.4	6.8	21.7
Internal secondary branch	15	5.0	–	7.1	14.3	–	19.6	6.1	18.0	0.6	1.3	5.6	17.9
Claw II heights													
External primary branch	20	7.0	–	8.8	21.0	–	26.6	8.0	24.3	0.5	1.5	7.9	25.2
External secondary branch	18	5.3	–	7.6	16.2	–	21.7	6.5	19.5	0.5	1.3	6.8	21.7
Internal primary branch	20	6.2	–	8.9	19.2	–	24.5	7.3	22.1	0.6	1.5	7.1	22.7
Internal secondary branch	19	5.0	–	7.0	16.3	–	20.1	6.1	18.6	0.5	1.2	6.3	20.1
Claw III heights													
External primary branch	20	7.5	–	9.8	21.5	–	28.3	8.2	24.9	0.6	1.7	8.2	26.2
External secondary branch	15	5.8	–	7.6	16.6	–	22.6	6.6	20.1	0.6	1.4	6.8	21.7
Internal primary branch	20	6.4	–	8.8	19.8	–	25.7	7.5	22.6	0.6	1.6	7.0	22.4
Internal secondary branch	17	5.3	–	7.4	16.2	–	20.9	6.1	18.7	0.6	1.3	6.2	19.8

Table 5. Cont.

Character	N	RANGE				Mean		SD		Holotype			
		μm		μm									
Claw IV heights													
Anterior primary branch	19	7.5	–	9.5	21.5	–	29.1	8.3	25.1	0.6	1.8	8.1	25.9
Anterior secondary branch	17	5.9	–	7.5	17.5	–	22.5	6.7	20.5	0.5	1.2	6.1	19.5
Posterior primary branch	18	8.0	–	10.1	22.6	–	30.6	9.0	27.2	0.6	2.0	8.5	27.2
Posterior secondary branch	12	6.2	–	7.9	19.2	–	22.8	7.2	21.4	0.5	1.0	7.0	22.4

Table 6. Measurements [in μm] of the eggs of *Mesobiotus marmoreus* sp. nov.; eggs mounted in Hoyer’s medium; process base/height ratio is expressed as percentage; N—number of eggs/structures measured, RANGE refers to the smallest and the largest structure among all measured specimens; SD—standard deviation.

Character	N	RANGE		Mean		SD
Egg bare diameter	7	63.4	–	69.6	67.0	2.4
Egg full diameter	7	77.9	–	82.2	80.0	1.4
Process height	27	5.6	–	8.8	6.9	0.9
Process base width	27	3.4	–	6.5	5.0	0.7
Process base/height ratio	27	59%	–	94%	73%	10%
Inter-process distance	27	1.5	–	3.3	2.3	0.4
Number of processes on the egg circumference	7	26	–	30	28.3	1.5

3.3.1. Material Examined

In total, 53 animals, 9 eggs mounted on microscope slides in Hoyer’s medium (some of the eggs were embryonated), 4 eggs fixed on an SEM stub (18.09) and 3 specimens were processed for DNA sequencing.

3.3.2. Type Locality

16°00′14″ N, 108°15′48″ E; 66 m asl: Vietnam, The Marble Mountains, south of Đà Nẵng, stone walkway, coll. Daniel Stec and Krzysztof Miler, August 2018.

3.3.3. Etymology

The species is named after the place where it was discovered, namely, The Marble Mountains, from Latin “marble” = “marmor”.

3.3.4. Type Depositories

The holotype with 7 paratypes (slide VN.055.06) and 27 paratypes (slides: VN.055.*, where the asterisk can be substituted by any of the following numbers: 05, 07–08) and 7 eggs (slides: VN.055.*: 01–02) are deposited at the Institute of Systematics and Evolution of Animals, Polish Academy of Sciences, Sławkowska 17, 31-016, Kraków, Poland;

Eighteen paratypes (slides: VN.055.*: 09–10), two eggs (slides: VN.055.*: 03–04) and an SEM stub: 18.09 are deposited at the Institute of Zoology and Biomedical Research, Jagiellonian University, Gronostajowa 9, 30-387, Kraków, Poland.

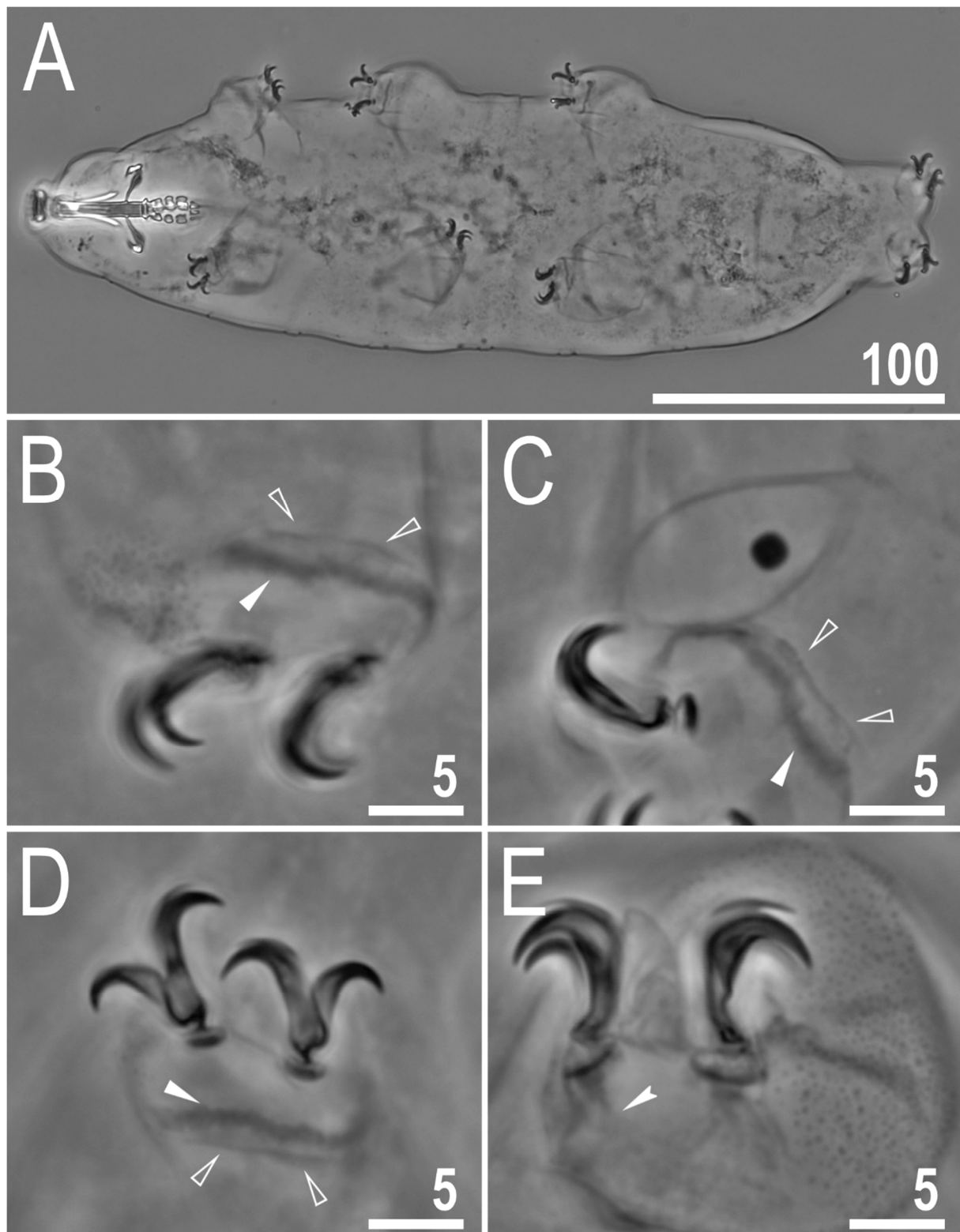


Figure 7. *Mesobiotus marmoreus* sp. nov.—PCM image of habitus and leg’s cuticle morphology and claws: (A)—dorso-ventral projection (holotype); (B)—granulation on the external surface of leg III (holotype); (C)—a pulvinus-like cuticular bulge on the internal surface of leg II (paratype); (D)—claws I with smooth lunulae (holotype); (E)—granulation on dorsal and lateral surface and claws on leg IV (paratype). Filled flat arrowheads indicate a single continuous cuticular bar above the claws, empty flat arrowheads indicate paired muscles attachments, filled indented arrowhead indicates horseshoe structure connecting the anterior and the posterior claw. Scale bars in μm .

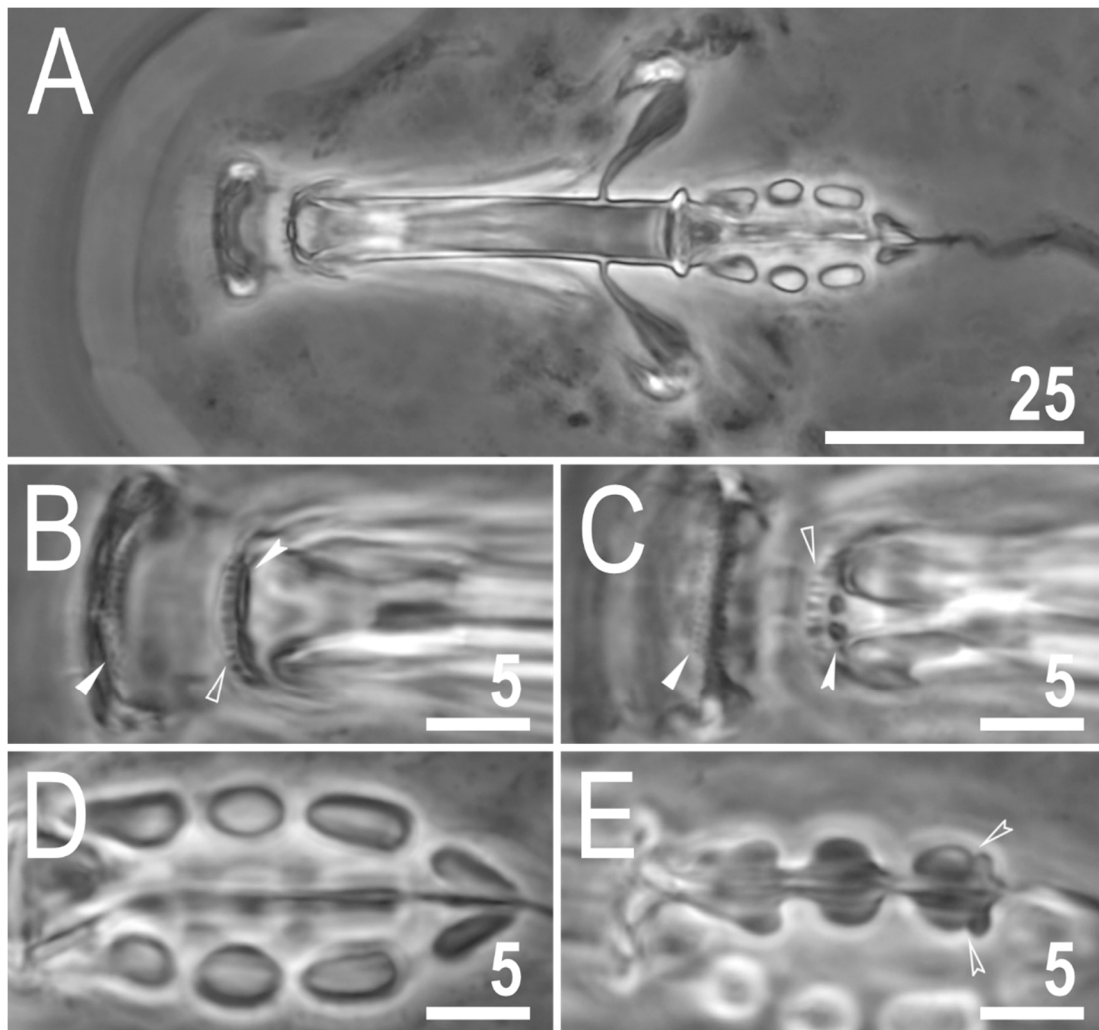


Figure 8. *Mesobiotus marmoreus* sp. nov.—PCM images of the buccal apparatus: (A)—an entire buccal apparatus (paratype); (B,C)—the oral cavity armature, dorsal and ventral teeth, respectively (paratype); (D,E)—placoid morphology, dorsal and ventral placoids, respectively (paratype). Filled flat arrowheads indicate the first band of teeth, empty flat arrowheads indicate the second band of teeth, filled indented arrowheads indicate the third band of teeth, empty indented arrowheads indicate subterminal constrictions in the third macroplacoid. Scale bars in μm .

3.3.5. Animals

The body is almost transparent in small specimens and whitish in adults; after fixation in Hoyer's medium, the body is transparent (Figure 7A). Eyes are absent in alive animals. The body cuticle is smooth, i.e., without pores or sculpturing. Granulation is present on the external surface of all legs I–III (Figure 7B) as well as on the lateral and dorsal surfaces of legs IV (Figure 1E). A cuticular bulge/fold, resembling a pulvinus, is present on the internal surface of legs I–III (Figure 7C). Claws are of the *Mesobiotus* type, with a peduncle connecting the claw to the lunula, a basal septum and well-developed accessory points situated in parallel to the primary branch (Figure 7D,E). Lunulae under all claws are smooth (Figure 7D,E). A single continuous cuticular bar and double muscle attachments are present above claws I–III (Figure 7B–D), whereas a horseshoe-shaped structure connects the anterior and posterior lunulae on claws IV (Figure 7E).

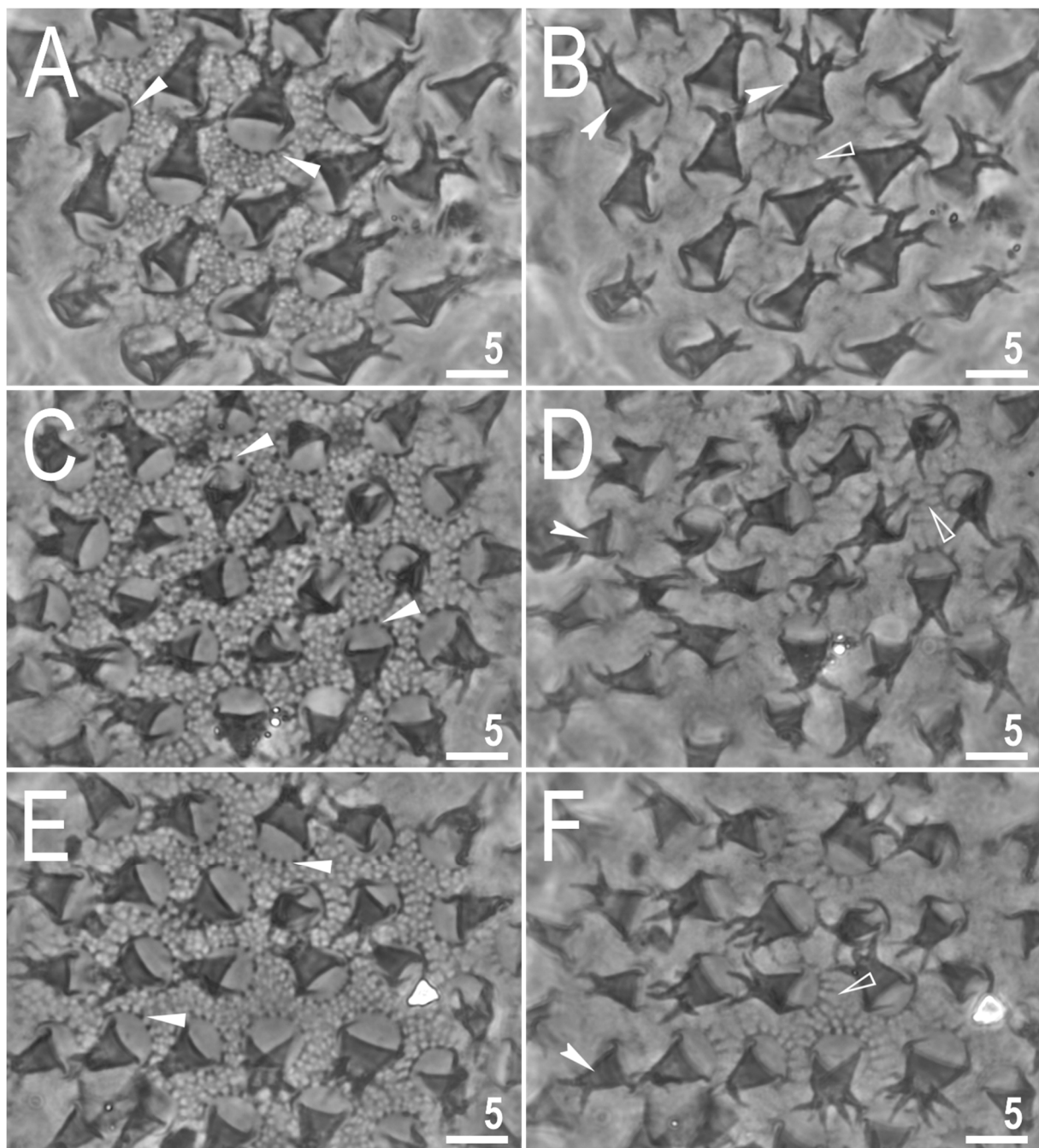


Figure 9. *Mesobiotus marmoreus* sp. nov.—PCM images of the egg surface under $\times 1000$ magnification. Each row represents a different egg whereas columns represent different focus levels. Filled flat arrowheads indicate crowns of thickenings around the process bases, empty flat arrowheads indicate extending striae radiating from processes bases, filled indented arrowheads indicate faint thickenings and darkening in processes trunk that in SEM are visible as annulations. Scale bars in μm .

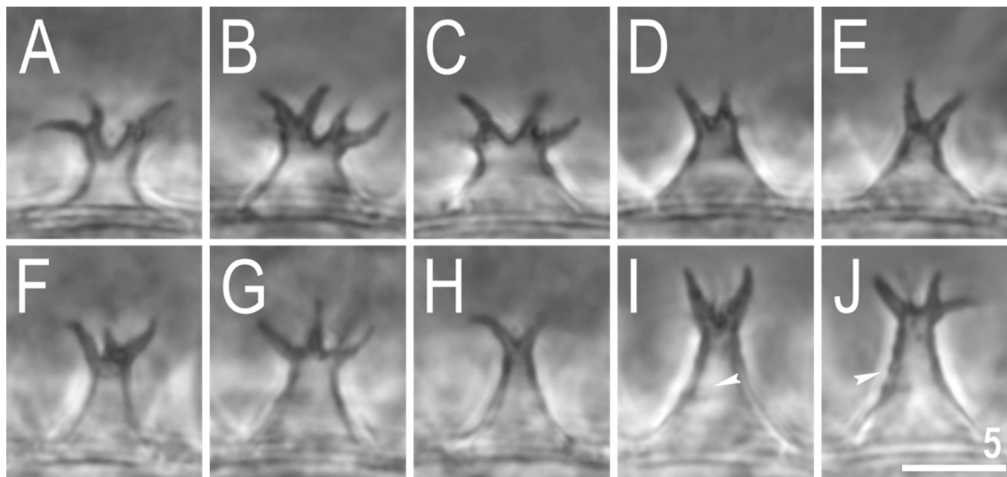


Figure 10. *Mesobiotus marmoreus* sp. nov.—PCM images of the egg processes midsections under $\times 1000$ magnification. Filled indented arrowheads indicate faint thickenings and darkening that in SEM are visible as annulations (see Figure 11). Scale bar in μm .

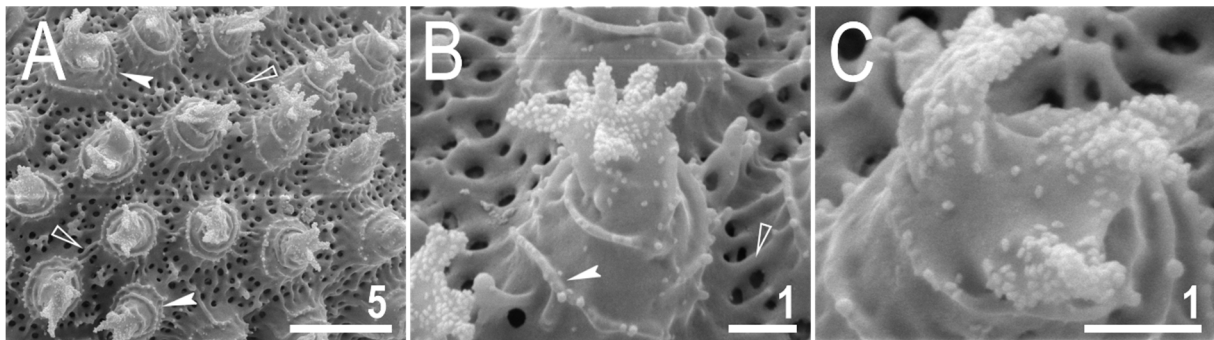


Figure 11. *Mesobiotus marmoreus* sp. nov.—SEM images of eggs: (A)—details of the egg surface; (B)—egg process; (C)—top part of the processes divided into several tentacular arms covered with fine granulation. Empty flat arrowheads indicate elevated bars of the reticulum that are visible as extending striae radiating from processes bases in PCM (see Figure 9), filled indented arrowheads indicate annulations present on the process trunks. Scale bars in μm .

The mouth is antero-ventral. The Bucco-pharyngeal apparatus is of the *Macrobiotus* type, with the ventral lamina and ten small peribuccal lamellae (Figure 8A). The oral cavity armature is well developed and composed of three bands of teeth (Figure 8B,C). The first band of teeth is composed of numerous small granules arranged in several discrete rows situated anteriorly in the oral cavity, just behind the bases of the peribuccal lamellae (Figure 8B,C). The second band of teeth is situated between the ring fold and the third band of teeth and is composed of ridges parallel to the main axis of the buccal tube that are larger than those in the first band (Figure 8B,C). The teeth of the third band are located within the posterior portion of the oral cavity, between the second band of teeth and the buccal tube opening (Figure 8B,C). The third band of teeth is discontinuous and divided into dorsal and ventral portions. Under PCM, dorsal teeth are visible as two lateral and one median transverse ridges/crests (Figure 8B) whereas ventral teeth consist of two lateral transverse ridges/crests between which two or three roundish and separated ventro-median teeth are present (Figure 8C). The pharyngeal bulb is ovoid (Figure 8A), with triangular apophyses, three rod-shaped macroplacoids and a large, elongated drop-shaped microplacoid placed close to the third macroplacoid (Figure 8D,E). The macroplacoid length sequence is $2 < 3 < 1$. The first macroplacoid is anteriorly narrowed and the third has a clearly defined sub-terminal constriction (Figure 8E). Measurements and statistics are presented in Table 5.

3.3.6. Eggs

The eggs are spherical, whitish and laid freely, with processes in the shape of cones with multiple apices (Figures 9–11). In PCM, the egg surface is covered with a fine but clearly visible reticulum, typically with 2–5 rows of meshes between the neighbouring processes (Figure 9A). In SEM, the egg surface appears between porous and reticulated states, with pores (0.2–0.5 μm in diameter) similar in size to the width of mesh nodes and bars (0.1–0.6 μm ; Figure 11A). In PCM, crowns of granular dark thickenings are present around the base of processes (Figure 9A,C,E), which extend into striae radiating from the process bases (Figure 9B,D,F). In SEM, these striae are also visible as elevated bars and nodes of the reticulum (Figure 11A,B). The egg processes exhibit one to three latitudinal annulations that are clearly visible only in SEM (Figure 11), whereas in PCM, they are only sometimes visible as faint, darkened lines in the process trunk (Figure 9B,D,F) or as faintly visible, thickening in the process midsection (Figure 10L,J). Under SEM, the annulations are seen as laminal rings with small granules present on their margins, giving the serrated impression (Figure 11). The process apex divided into multiple (typically 3–6), slender, varying in length, tentacular arms (Figures 9–11), which are covered by fine granulation, visible only in SEM (Figure 11). Measurements and statistics are presented in Table 6.

3.3.7. Reproduction

The examination of all individuals, freshly mounted in Hoyer's medium, under PCM has not revealed any testis or spermathecae filled with spermatozoa. Thus, it is most likely that the new species is parthenogenetic.

3.3.8. DNA Sequences

The obtained sequences for all four molecular markers analysed in this study were of good quality and were represented by single haplotypes.

The **18S rRNA** sequences (GenBank: OL257856-8), 1009 bp long.

The **28S rRNA** sequences (GenBank: OL257868-70), 799 bp long.

The **ITS-2** sequences (GenBank: OL257861-3), 405 bp long.

The **COI** sequences (GenBank: OL311516-8), 658 bp long;

3.4. Phylogenetic Position of the New Taxa

The phylogenetic analysis of taxa belonging to the genus *Mesobiotus* did not indicate *M. harmsworthi* and *M. furciger* groups to be monophyletic (Figure 12). Species representing each of these groups are intermixed in the obtained tree (Figure 12). The analysis indicated *Mesobiotus imperialis* **sp. nov.** is closely related to *Mesobiotus philippinicus* (Figure 12). This is also obvious when inspecting the genetic distances that show a large amount of similarity between DNA sequences of nuclear markers (p-distance; 18S rRNA: 0.0%, 28S rRNA: 2.3%; SM.05). The same occurred in case of the COI dataset, where the lowest genetic distance out of all comparisons with other *Mesobiotus* taxa was 16.5% (p-distance; SM.05). In the tree, the closest relative of *Mesobiotus marmoreus* **sp. nov.** is *Mesobiotus dilimanensis* Itang, Stec, Mapalo Mirano-Bascos & Michalczyk, 2020 [50] (Figure 12). The genetic distances between these two species are also the lowest out of all conducted comparisons (p-distance; 18S rRNA: 0.1%, 28S rRNA: 1.5%, ITS-2: 9.9%, COI: 21.1%; SM.05).

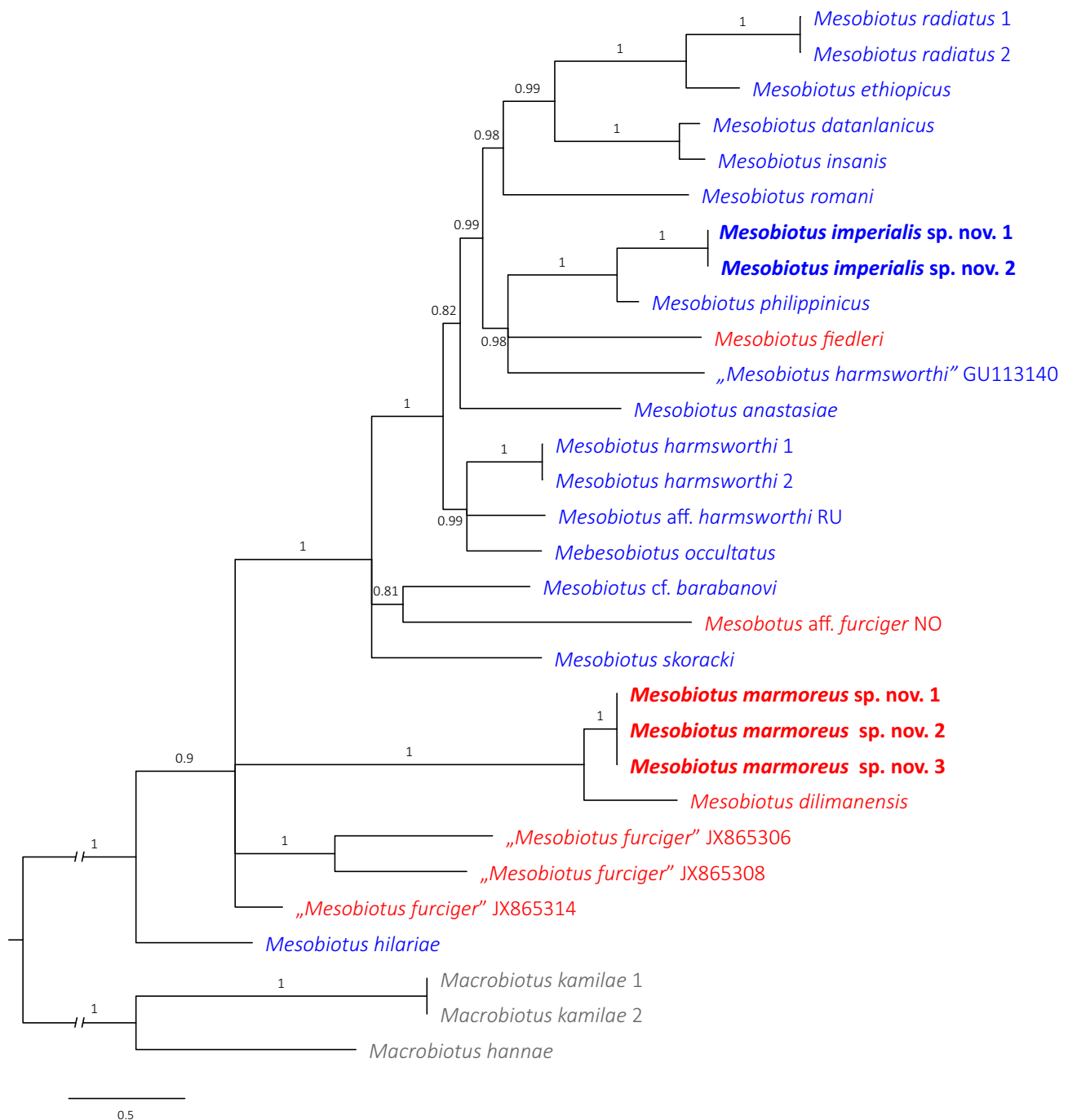


Figure 12. The Bayesian Inference (BI) phylogeny constructed from concatenated sequences (18S rRNA + 28S rRNA + ITS-2 + COI) of the genus *Mesobiotus*. Numbers at nodes indicate Bayesian posterior probability; nodes with values below 0.80 have been collapsed. Taxa newly sequenced in this study are marked with bolded font. Taxa of the *M. harmsworthi* and *M. furciger* complex are indicated by blue and red font, respectively. Outgroup is indicated by grey font. Quotation marks indicate misidentified *Mesobiotus* species or species with uncertain species identification. Scale bar represents substitutions per position.

4. Discussion

4.1. Differential Diagnosis of *Mesobiotus imperialis* sp. nov.

The new species belong to the informal *Mesobiotus harmsworthi* morphogroup as it exhibits rather large conical processes. After using the dichotomous key by Kaczmarek et al. [7] and Tumanov [8], the new species have been identified as *Mesobiotus philippinicus* known only from its type locality in Philippines [30]. Importantly, it should be also noted that both men-

tioned keys contain a mistake saying that *M. philippinicus* has the first band of teeth in the oral cavity armature not visible in light microscopy, which is not true [30]. However, despite the phenotypic match, the genetic data and phylogenetic analysis clearly indicate the Vietnamese population to be a distinct species. Closer comparison revealed minute morphological and morphometric differences based on which the new species is differentiated.

Mesobiotus imperialis **sp. nov.** differs from *M. philippinicus* by the presence of granulation on all legs that is visible in light microscopy (only granulation on leg IV faintly visible in some specimens of *M. philippinicus*), evidently more pronounced thickenings surrounding the bases of egg processes in the new species (crown of thickenings surrounding processes bases less pronounced in *M. philippinicus*), unevenly distributed depressions and faint tubercles in the egg processes walls (processes walls are smooth, without mentioned depressions and tubercles in *M. philippinicus*, with this character observable only in SEM), and having conical processes always stretched (egg processes covered with wrinkles forming a rose-like whorl in *M. philippinicus*; *remark*: Based on personal observations, this character is most probably an artefact caused by the culture environment and, importantly, *M. philippinicus* was described based on specimens from laboratory isolate). The morphometric comparisons of both populations revealed that ranges of measured characters greatly overlap. Therefore, statistical testing was involved to check for eventual differences between analysed species. T-test comparisons of morphometric characters revealed statistically significant differences between these two populations in almost all absolute and all relative claws measurements, with claws being larger in *M. philippinicus* ($p_{B-H} \ll 0.002$; SM.03). Out of the remaining animals' measurements, *pt* values for stylet support insertion point as well as ventral lamina length were also significantly different and larger in *M. philippinicus* and the new species, respectively ($p_{B-H} \ll 0.002$; SM.03). Moreover, there were also significant differences in egg measurements such as egg bare diameter, process height, process base–height ratio and inter-process distances ($p_{B-H} \ll 0.007$; SM.03). Nevertheless, as stated above, these latter differences in egg dimensions should be treated with great caution as they might be caused by culturing conditions.

4.2. Differential Diagnosis of *Mesobiotus marmoreus* sp. nov.

The new species belongs to the informal *Mesobiotus furciger* morphogroup as it exhibits rather small conical processes with branched apices. After using the dichotomous key by Kaczmarek et al. [7] and Tumanov [8], the new species could not be identified. By having reticulated egg surface between processes (at least visible as such in light microscopy) the new species is similar to the following taxa: *Mesobiotus creber* (Pilato & Lisi, 2009) [63], *M. dilimanensis*, *Mesobiotus divergens* (Binda, Pilato & Lisi, 2005) [64], *Mesobiotus kovalevi* (Tumanov, 2004) [65] and *Mesobiotus siamensis* (Tumanov, 2006) [66], but it differs specifically from the following:

Mesobiotus creber known only from the Seychelles Islands [63] by the presence of granulation on all legs (the granulation absent in *M. creber*); the medio-ventral tooth of the third band of teeth usually subdivided into three roundish teeth (only up to two roundish teeth present in *M. creber*); a more anteriorly positioned stylet support insertion point ($pt = 76.2\text{--}77.8$ in the new species vs. $pt = 80.0\text{--}80.9$ in *M. creber*); a more evident subdivisions of process apices that resemble tentacular arms (process apices subdivided into short, nodular terminal branches in *M. creber*); a larger egg bare diameter (63.4–69.6 μm in the new species vs. 52–60 μm in *M. creber*); a larger egg full diameter (77.9–82.2 μm in the new species vs. 59–66 μm in *M. creber*).

Mesobiotus dilimanensis, known only from the Philippines [50], by a different macroplacoid sequence ($2 < 3 < 1$ in the new species vs. $2 < 1 = 3$ in *M. dilimanensis*); a more anteriorly positioned stylet support insertion point ($pt = 76.2\text{--}77.8$ in the new species vs. $pt = 78.0\text{--}81.4$ in *M. dilimanensis*); longer primary branches of external claws I (6.4–8.6 μm in the new species vs. 8.8–12.1 μm in *M. dilimanensis*); longer primary branches of external and internal claws II (7.0–8.8 and 6.2–8.9 μm , respectively in the new species vs. 10.0–12.9 and 9.2–12.0 μm , respectively in *M. dilimanensis*); longer primary branches of anterior and

posterior claws IV (7.5–9.5 and 8.0–10.1 μm , respectively in the new species vs. 9.7–14.8 and 10.7–14.8 μm , respectively in *M. dilimanensis*); the presence of subdivisions in processes apices that resemble slender tentacular arms (process apices subdivided into multiple short, nodular, finger-like apices in *M. dilimanensis*); the presence of one to three latitudinal annulations on the processes trunks that are seen as laminal rings with small granules present on their margins giving the serrated impression (small globular tubercles present on the processes trunks in *M. dilimanensis*); a larger number of processes on the egg circumference (26–30 in the new species vs. 18–24 in *M. dilimanensis*).

Mesobiotus divergens, known only from New Zealand [64], by the presence of granulation on all legs (the granulation absent in *M. divergens*); the morphology of the stylet sheaths (typical in the new species vs. caudally thickened lateral portions of stylet sheaths in *M. divergens*); a relatively longer placoid row ($pt = 53.7\text{--}61.2$ in the new species vs. $pt = 45.4\text{--}51.6$ in *M. divergens*); a relatively larger microplacoid ($pt = 9.6\text{--}12.7$ in the new species vs. $pt = 7.1\text{--}7.4$ in *M. divergens*); a larger number of processes on the egg circumference (26–30 in the new species vs. 17 in *M. divergens*); a different point of division of the egg process apex (division closer to the process tip in the new species vs. division at half of the process height in *M. divergens*); the presence of subdivisions in process apices that resemble slender tentacular arms (processes subdivided into two or three stout branches that might be further subdivided into multiple, finger-like, nodular apices in *M. divergens*).

Mesobiotus kovalevi, known only from New Zealand [65], by the absence of eyes; the presence of granulation on all legs (the granulation absent in *M. kovalevi*); the presence of three bands of teeth in the oral cavity (the first and the second band of teeth absent or invisible in light microscopy in *M. kovalevi*); the presence of a medio ventral tooth of the third band of teeth subdivided into two or three roundish teeth (a single roundish medio-ventral tooth present in *M. kovalevi*); a different morphology of egg processes (in light microscopy stout processes with smooth trunks and apices divided into multiple slender, tentacular arms in the new species vs. elongated, conical processes only sometimes subdivided at the top with trunks covered with irregularly distributed minute spines in *M. kovalevi*); a smaller egg bare diameter (63.4–69.6 μm in the new species vs. 86–95 μm in *M. kovalevi*); shorter egg processes (5.6–8.8 μm in the new species vs. 12–17 μm in *M. kovalevi*), a slightly larger number of processes on the egg circumference (26–30 in the new species vs. up to 25 in *M. kovalevi*); a smaller meshes in the reticulum covering the egg surface between processes (meshes diameter 0.2–0.5 μm in the new species vs. nearly 1 μm in *M. kovalevi*).

Mesobiotus siamensis, known only from Thailand [66], by the presence of granulation on all legs (the granulation absent in *M. siamensis*); a more-developed first band of teeth in the oral cavity (always clearly visible in light microscopy in the new species vs. barely visible even in largest specimens of *M. siamensis*); the presence of a medio-ventral tooth of the third band of teeth subdivided into two or three roundish teeth (a medio-ventral tooth only almost broken into several granules in *M. siamensis*); a different morphology of lunulae IV (smooth in the new species vs. with undulated margins in *M. siamensis*); a different morphology of egg processes (in light microscopy stout processes with smooth trunks and apices divided into multiple slender, tentacular arms in the new species vs. bottle-shaped processes with an evidently elongated distal part that is subdivided at the top into short and pointed apices in *M. siamensis*); shorter processes (5.6–8.8 μm in the new species vs. 10.7–11.8 μm in *M. siamensis*); narrower process bases (3.4–6.5 μm in the new species vs. 7.4–10.0 μm in *M. siamensis*); a smaller egg bare diameter (63.4–69.6 μm in the new species vs. 70.3–77.7 μm in *M. siamensis*); a larger number of processes on the egg circumference (26–30 in the new species vs. up to 22 in *M. siamensis*).

4.3. Conclusions

Thanks to the integrative analysis of the two newly found *Mesobiotus* populations and their descriptions, as new to science, the number of Vietnamese tardigrade species was elevated to 36. The two new taxa presented herein have their closest relatives in Philippines as recovered by phylogenetic analysis also reflected in morphological similarities. This

finding is not surprising when considering the geographic distance and the fact that both these regions belong to the generally speaking Oriental zoogeographic realm. Therefore, the more recent split of these evolutionary lineages should have been expected.

Supplementary Materials: The following are available online at <https://www.mdpi.com/article/10.3390/d13110605/s1>, SM.01. Raw morphometric data of *Mesobiotus imperialis* sp. nov. SM.02. Raw morphometric data of *Mesobiotus marmoreus* sp. nov. SM.03. Results of T-test comparisons. SM.04. Best-fit partitioning scheme and models suggested by PartitionFinder. SM.05. Uncorrected pairwise genetic distances.

Funding: The study was supported by the *Preludium* programme of the National Science Centre, Poland (grant no. 2018/31/N/NZ8/03096 to DS). During this study, DS was supported by the Foundation for Polish Science (FNP).

Institutional Review Board Statement: Not applicable.

Data Availability Statement: The author confirms that the data supporting the findings of this study are available within the article and its Supplementary Materials. The DNA sequences generated in this study are available in GenBank.

Acknowledgments: I am especially grateful to Krzysztof Miler for his magnificent help with samples collection.

Conflicts of Interest: The author declares no conflict of interest.

References

- Nelson, D.R.; Guidetti, R.; Rebecchi, L. Phylum Tardigrada. In *Ecology and General Biology*, 4th ed.; Thorp, J., Rogers, D.C., Eds.; Thorp and Covich's Freshwater Invertebrates; Academic Press Inc.: Cambridge, MA, USA, 2015; Volume 1, pp. 347–380. [[CrossRef](#)]
- Guidetti, R.G.; Bertolani, R.B. Tardigrade taxonomy: An updated check list of the taxa and a list of characters for their identification. *Zootaxa* **2005**, *845*, 1–46. [[CrossRef](#)]
- Degma, P.; Guidetti, R. Notes to the current checklist of Tardigrada. *Zootaxa* **2007**, *1579*, 41–53. [[CrossRef](#)]
- Degma, P.; Bertolani, R.; Guidetti, R. Actual Checklist of Tardigrada Species. Available online: https://doi.org/10.25431/11380_178608 (accessed on 26 April 2021).
- Vecchi, M.; Cesari, M.; Bertolani, R.; Jönsson, K.I.; Rebecchi, L.; Guidetti, R. Integrative systematic studies on tardigrades from Antarctica identify new genera and new species within Macrobiotidea and Echiniscoidea. *Invertebr. Syst.* **2016**, *30*, 303–322. [[CrossRef](#)]
- Stec, D.; Vecchi, M.; Calhim, S.; Michalczyk, Ł. New multilocus phylogeny reorganises the family Macrobiotidae (Eutardigrada) and unveils complex morphological evolution of the *Macrobiotus hufelandi* group. *Mol. Phylogenetics Evol.* **2020**, *160*, 106987. [[CrossRef](#)] [[PubMed](#)]
- Kaczmarek, Ł.; Bartylak, T.; Stec, D.; Kulpa, A.; Kepel, M.; Kepel, A.; Roszkowska, M. Revisiting the genus *Mesobiotus* Vecchi et al. 2016 (Eutardigrada, Macrobiotidae)—remarks, updated dichotomous key and an integrative description of new species from Madagascar. *Zoöl. Anz. A J. Comp. Zoöl.* **2020**, *287*, 121–146. [[CrossRef](#)]
- Tumanov, D.V. Integrative description of *Mesobiotus anastasiae* sp. nov. (Eutardigrada, Macrobiotidea) and first record of Loboalacarus (Chelicerata, Trombidiformes) from the Republic of South Africa. *Eur. J. Taxon.* **2020**, *726*, 102–131. [[CrossRef](#)]
- Kaczmarek, Ł.; Zawierucha, K.; Buda, J.; Stec, D.; Gawlak, M.; Michalczyk, Ł.; Roszkowska, M. An integrative redescription of the nominal taxon for the *Mesobiotus harmsworthi* group (Tardigrada: Macrobiotidae) leads to descriptions of two new *Mesobiotus* species from Arctic. *PLoS ONE* **2018**, *13*, e0204756. [[CrossRef](#)]
- Węglarska, B. Die Tardigraden Vietnams. *Acta Soc. Zool. Bohemoslov.* **1962**, *26*, 300–307.
- Iharos, G. Einige Angaben zur Tardigradenfauna Vietnams. *Opusc. Zool. Bp.* **1969**, *9*, 273–277.
- Pilato, G.; Binda, M.G. Isohypsibius barbarae, a new species of eutardigrade from Vietnam. *Bolletino Delle Sedute Dell'accademia Gioenia Di Sci. Nat. Catania* **2002**, *35*, 637–642.
- Beasley, C.W.; Kaczmarek, Ł.; Michalczyk, Ł. Redescription of *Doryphoribius vietnamensis* (Iharos, 1969) comb. nov. on the basis of the holotype and additional material from China. *Acta Zool. Acad. Sci. Hung.* **2006**, *52*, 367–372. [[CrossRef](#)]
- Tchesunov, A.V. Marine tardigrade *Halechiniscus jejuensis* Chang et Rho, 2002 (Arthrotardigrada: Halechiniscidae) found in Vietnam. *Invertzool* **2011**, *8*, 79–85. [[CrossRef](#)]
- Stec, D. *Mesobiotus datanlanicus* sp. nov., a new tardigrade species (Macrobiotidae: *Mesobiotus harmsworthi* group) from Lâm Đồng Province in Vietnam. *Zootaxa* **2019**, *4679*, 164–180. [[CrossRef](#)] [[PubMed](#)]
- Gąsiorek, P.; Vončina, K.; Nelson, D.R.; Michalczyk, Ł. The importance of being integrative: A remarkable case of synonymy in the genus *Viridiscus* (Heterotardigrada: Echiniscidae). *Zool. Lett.* **2021**, in press. [[CrossRef](#)]
- Murray, J. XXV.—Arctic Tardigrada, collected by Wm. S. Bruce. *Trans. R. Soc. Edinb.* **1907**, *45*, 669–681. [[CrossRef](#)]

18. Stec, D.; Smolak, R.; Kaczmarek, Ł.; Michalczyk, Ł. An integrative description of *Macrobiotus paulinae* sp. nov. (Tardigrada: Eutardigrada: Macrobiotidae: Hufelandi group) from Kenya. *Zootaxa* **2015**, *4052*, 501–526. [[CrossRef](#)] [[PubMed](#)]
19. Morek, W.; Stec, D.; Gąsiorek, P.; Schill, R.O.; Kaczmarek, Ł.; Michalczyk, Ł. An experimental test of eutardigrade preparation methods for light microscopy. *Zoöl. J. Linn. Soc.* **2016**, *178*, 785–793. [[CrossRef](#)]
20. Coughlan, K.; Stec, D. Two new species of the *Macrobiotus hufelandi* complex (Tardigrada: Eutardigrada: Macrobiotidae) from Australia and India, with notes on their phylogenetic position. *Eur. J. Taxon.* **2019**, *573*, 1–38. [[CrossRef](#)]
21. Coughlan, K.; Michalczyk, Ł.; Stec, D. *Macrobiotus caelestis* sp. nov., a New Tardigrade Species (Macrobiotidae: Hufelandi Group) from the Tien Shan Mountains (Kyrgyzstan). *Ann. Zoöl.* **2019**, *69*, 499. [[CrossRef](#)]
22. Stec, D.; Gąsiorek, P.; Morek, W.; Koszytła, P.; Zawierucha, K.; Michno, K.; Kaczmarek, Ł.; Prokop, Z.M.; Michalczyk, Ł. Estimating optimal sample size for tardigrade morphometry. *Zoöl. J. Linn. Soc.* **2016**, *178*, 776–784. [[CrossRef](#)]
23. Pilato, G.; Binda, M.G. Definition of families, subfamilies, genera and subgenera of the Eutardigrada, and keys to their identification. *Zootaxa* **2010**, *2404*, 1–54. [[CrossRef](#)]
24. Michalczyk, Ł.; Kaczmarek, Ł. A description of the new tardigrade *Macrobiotus reinhardti* (Eutardigrada: Macrobiotidae, harmsworthi group) with some remarks on the oral cavity armature within the genus *Macrobiotus* Schultze. *Zootaxa* **2003**, *331*, 1–24. [[CrossRef](#)]
25. Kaczmarek, Ł.; Michalczyk, Ł. The *Macrobiotus hufelandi* group (Tardigrada) revisited. *Zootaxa* **2017**, *4363*, 101–123. [[CrossRef](#)]
26. Kaczmarek, Ł.; Cytan, J.; Zawierucha, K.; Diduszko, D.; Michalczyk, Ł. Tardigrades from Peru (South America), with descriptions of three new species of Parachela. *Zootaxa* **2014**, *3790*, 357–379. [[CrossRef](#)]
27. Kiosya, Y.; Pogwizd, J.; Matsko, Y.; Vecchi, M.; Stec, D. Phylogenetic position of two *Macrobiotus* species with a revisional note on *Macrobiotus sottilei* Pilato, Kiosya, Lisi & Sabella, 2012 (Tardigrada: Eutardigrada: Macrobiotidae). *Zootaxa* **2021**, *4933*, 113–135. [[CrossRef](#)]
28. Pilato, G. Analisi di nuovi caratteri nello studio degli Eutardigradi. *Animalia* **1981**, *8*, 51–57.
29. Michalczyk, Ł.; Kaczmarek, Ł. The Tardigrada Register: A comprehensive online data repository for tardigrade taxonomy. *J. Limnol.* **2013**, *72*, e22. [[CrossRef](#)]
30. Mapalo, M.A.; Stec, D.; Mirano-Bascos, D.; Michalczyk, Ł. *Mesobiotus philippinicus* sp. nov., the first limnoterrestrial tardigrade from the Philippines. *Zootaxa* **2016**, *4126*, 411–426. [[CrossRef](#)]
31. R Core Team. *R: A Language and Environment for Statistical Computing*; R Foundation for Statistical Computing: Vienna, Austria, 2021; Available online: <http://www.R-project.org/> (accessed on 26 April 2021).
32. Benjamini, Y.; Hochberg, Y. Controlling the False Discovery Rate: A Practical and Powerful Approach to Multiple Testing. *J. R. Stat. Soc. Ser. B Methodol.* **1995**, *57*, 289–300. [[CrossRef](#)]
33. Casquet, J.; Thébaud, C.; Gillespie, R.G. Chelex without boiling, a rapid and easy technique to obtain stable amplifiable DNA from small amounts of ethanol-stored spiders. *Mol. Ecol. Resour.* **2011**, *12*, 136–141. [[CrossRef](#)] [[PubMed](#)]
34. Stec, D.; Kristensen, R.M.; Michalczyk, Ł. An integrative description of *Minibiotus ioculator* sp. nov. from the Republic of South Africa with notes on *Minibiotus pentannulatus* Londoño et al., 2017 (Tardigrada: Macrobiotidae). *Zoöl. Anz. A J. Comp. Zoöl.* **2020**, *286*, 117–134. [[CrossRef](#)]
35. Hall, T.A. BioEdit: A user-friendly biological sequence alignment editor and analysis program for Windows 95/98/NT. *Nucleic Acids Symp. Ser.* **1999**, *41*, 95–98.
36. Kumar, S.; Stecher, G.; Tamura, K. MEGA7: Molecular Evolutionary Genetics Analysis Version 7.0 for Bigger Datasets. *Mol. Biol. Evol.* **2016**, *33*, 1870–1874. [[CrossRef](#)]
37. Stec, D.; Zawierucha, K.; Michalczyk, Ł. An integrative description of *Ramazzottius subanomalus* (Biserov, 1985) (Tardigrada) from Poland. *Zootaxa* **2017**, *4300*, 403–420. [[CrossRef](#)]
38. Gąsiorek, P.; Stec, D.; Zawierucha, K.; Kristensen, R.M.; Michalczyk, Ł. Revision of *Testechiniscus* Kristensen, 1987 (Heterotardigrada: Echiniscidae) refutes the polar-temperate distribution of the genus. *Zootaxa* **2018**, *4472*, 261–297. [[CrossRef](#)]
39. Mironov, S.V.; Dabert, J.; Dabert, M. A new feather mite species of the genus *Proctophyllodes* Robin, 1877 (Astigmata: Proctophyllodidae) from the Long-tailed Tit *Aegithalos caudatus* (Passeriformes: Aegithalidae)—morphological description with DNA barcode data. *Zootaxa* **2012**, *3253*, 54–61. [[CrossRef](#)]
40. Stec, D.; Morek, W.; Gąsiorek, P.; Michalczyk, Ł. Unmasking hidden species diversity within the *Ramazzottius oberhaeuseri* complex, with an integrative redescription of the nominal species for the family Ramazzottiidae (Tardigrada: Eutardigrada: Parachela). *Syst. Biodivers.* **2018**, *16*, 357–376. [[CrossRef](#)]
41. Astrin, J.J.; Stüben, P.E. Phylogeny in cryptic weevils: Molecules, morphology and new genera of western Palaearctic Cryptorhynchinae (Coleoptera:Curculionidae). *Invertebr. Syst.* **2008**, *22*, 503–522. [[CrossRef](#)]
42. Nowak, B. An integrative description of *Macrobiotus hanna* sp. nov. (Tardigrada: Eutardigrada: Macrobiotidae: Hufelandi group) from Poland. *Turk. J. Zoöl.* **2018**, *42*, 269–286. [[CrossRef](#)]
43. Katoh, K.; Misawa, K.; Kuma, K.; Miyata, T. MAFFT: A novel method for rapid multiple sequence alignment based on fast Fourier transform. *Nucleic Acids Res.* **2002**, *30*, 3059–3066. [[CrossRef](#)]
44. Katoh, K.; Toh, H. Recent developments in the MAFFT multiple sequence alignment program. *Briefings Bioinform.* **2008**, *9*, 286–298. [[CrossRef](#)]
45. Vaidya, G.; Lohman, D.J.; Meier, R. SequenceMatrix: Concatenation software for the fast assembly of multi-gene datasets with character set and codon information. *Cladistics* **2011**, *27*, 171–180. [[CrossRef](#)]

46. Lanfear, R.; Frandsen, P.B.; Wright, A.M.; Senfeld, T.; Calcott, B. PartitionFinder 2: New Methods for Selecting Partitioned Models of Evolution for Molecular and Morphological Phylogenetic Analyses. *Mol. Biol. Evol.* **2017**, *34*, 772–773. [[CrossRef](#)]
47. Ronquist, F.; Huelsenbeck, J.P. MrBayes 3: Bayesian phylogenetic inference under mixed models. *Bioinformatics* **2003**, *19*, 1572–1574. [[CrossRef](#)] [[PubMed](#)]
48. Rambaut, A.; Drummond, A.J. Tracer v1.6. 2014. Available online: <http://beast.bio.ed.ac.uk/Tracer> (accessed on 8 September 2021).
49. Stec, D.; Kristensen, R.M. An integrative description of *Mesobiotus ethiopicus* sp. nov. (Tardigrada: Eutardigrada: Parachela: Macrobiotidae: Harmsworthi group) from the northern Afrotropic region. *Turk. J. Zool.* **2017**, *41*, 800–811. [[CrossRef](#)]
50. Itang, L.A.M.; Stec, D.; Mapalo, M.A.; Mirano-Bascos, D.; Michalczyk, Ł. An integrative description of *Mesobiotus dilimanensis*, a new tardigrade species from the Philippines (Eutardigrada: Macrobiotidae: Furciger group). *Raffles Bull. Zool.* **2020**, *68*, 19–31.
51. Mapalo, M.; Stec, D.; Mirano-Bascos, D.; Michalczyk, Ł. An integrative description of a limnoterrestrial tardigrade from the Philippines, *Mesobiotus insanis*, new species (Eutardigrada: Macrobiotidae: Harmsworthi group). *Raffles Bull. Zool.* **2017**, *65*, 440–454.
52. Pilato, G.; Binda, M.G.; Catanzaro, R. Remarks on some tardigrades of the African fauna with the description of three new species of *Macrobiotus* Schultze 1834. *Trop. Zool.* **1991**, *4*, 167–178. [[CrossRef](#)]
53. Stec, D.; Roszkowska, M.; Kaczmarek, Ł.; Michalczyk, Ł. An integrative description of a population of *Mesobiotus radiatus* (Pilato, Binda & Catanzaro, 1991) from Kenya. *Turk. J. Zool.* **2018**, *42*, 523–540. [[CrossRef](#)]
54. Roszkowska, M.; Stec, D.; Gawlak, M.; Kaczmarek, Ł. An integrative description of a new tardigrade species *Mesobiotus romani* sp. nov. (Macrobiotidae: Harmsworthi group) from the Ecuadorian Pacific coast. *Zootaxa* **2018**, *4450*, 550–564. [[CrossRef](#)]
55. Murray, J. Encystment of Tardigrada. *Trans. R. Soc. Edinb.* **1908**, *45*, 837–854. [[CrossRef](#)]
56. Czechowski, P.; Sands, C.J.; Adams, B.J.; D’Haese, C.A.; Gibson, J.A.E.; McInnes, S.J.; Stevens, M.I. Antarctic Tardigrada: A first step in understanding molecular operational taxonomic units (MOTUs) and biogeography of cryptic meiofauna. *Invertebr. Syst.* **2012**, *26*, 526–538. [[CrossRef](#)]
57. Kayastha, P.; Roszkowska, M.; Mioduchowska, M.; Gawlak, M.; Kaczmarek, Ł. Integrative Descriptions of Two New Tardigrade Species along with the New Record of *Mesobiotus skorackii* Kaczmarek et al., 2018 from Canada. *Diversity* **2021**, *13*, 394. [[CrossRef](#)]
58. Doyère, P.L.N. Memoire sur les Tardigrades. *Ann. Des Sci. Nat.* **1840**, *14*, 269–362.
59. Richters, F. Tardigrada. In *Handbuch der Zoologie*; Kükenthal, W., Krumbach, T., Eds.; Walter de Gruyter & Co.: Berlin/Heidelberg, Germany, 1926; Volume 3, pp. 58–61.
60. Schuster, R.O.; Nelson, D.R.; Grigarick, A.A.; Christenberry, D. Systematic Criteria of the Eutardigrada. *Trans. Am. Microsc. Soc.* **1980**, *99*, 284–303. [[CrossRef](#)]
61. Thulin, G. Über die phylogenie und das system der tardigraden. *Hereditas* **2010**, *11*, 207–266. [[CrossRef](#)]
62. Marley, N.; McInnes, S.J.; Sands, C. Phylum Tardigrada: A re-evaluation of the Parachela. *Zootaxa* **2011**, *2819*, 51–64. [[CrossRef](#)]
63. Pilato, G.; Lisi, O.P.V. Tardigrades of the Seychelles Islands, with the description of three new species. *Zootaxa* **2009**, *2124*, 1–20. [[CrossRef](#)]
64. Binda, M.G.; Pilato, G.; Lisi, O.P.V. Remarks on *Macrobiotus furciger* Murray, 1906 and description of three new species of the furciger group (Eutardigrada, Macrobiotidae). *Zootaxa* **2005**, *1075*, 55–68. [[CrossRef](#)]
65. Tumanov, D.V. *Macrobiotus kovalevi*, a new species of Tardigrada from New Zealand (Eutadigrada, Macrobiotidae). *Zootaxa* **2004**, *406*, 1–8. [[CrossRef](#)]
66. Tumanov, D.V. *Macrobiotus siamensis* sp. n. (Eutardigrada, Macrobiotidae) from Thailand (Asia). *Zootaxa* **2006**, *1202*, 53–59. [[CrossRef](#)]